USAATCOM TR 95-D-9

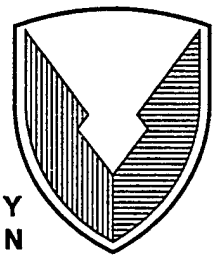

U.S. ARMY
AVIATION
AND TROOP COMMAND

DEVELOPMENT OF A SYSTEM FOR IMPROVED HELICOPTER BLADE TRACKING

Richard L. Bielawa and Kirk Frederickson

Renasselaaer Polytechnic Institute
110 8th Street
Troy, NY 12180-3590

June 1995

Final Report

Approved for public release; distribution unlimited.

Prepared for:

AVIATION APPLIED TECHNOLOGY DIRECTORATE
U.S. ARMY AVIATION AND TROOP COMMAND
FORT EUSTIS, VA 23604-5577

AVIATION APPLIED TECHNOLOGY DIRECTORATE
POSITION STATEMENT

This report presents the results of a demonstration of an experimental method of determining the flapping moment of inertia of a helicopter rotor blade. The purpose of the work was to validate an approach to measure a parameter which is thought to be a measure of manufacturing quality which relates directly to the blades ability to be flown with minimum vibration without extensive (and costly) adjustment. The accuracy of the method was demonstrated first for a simple prismatic bar. Measurements were then made on UH-60 Black Hawks' recently manufactured blades and a blade with a small mass added. The calculated and empirically estimated flapping moments of inertia for the prismatic bar were in excellent agreement. Calculated and experimentally determined flapping moments of inertia for the UH-60 Black Hawk blades were in satisfactory agreement. The experimental method was shown to be both precise and repeatable. The results presented in the report will serve as the basis for establishing a more production-oriented quality test procedure which could be used for new or repaired main rotor blades to reduce the number of tracking flights required to obtain satisfactory vibration characteristics.

The project engineers for this effort were, in succession, David Kinney and Edward Austin of the Air Vehicle Structures Division.

REPORT DOCUMENTATION PAGE

Form Approved
OMB No. 0704-0188

1. AGENCY USE ONLY (Leave blank)	2. REPORT DATE	3. REPORT TYPE AND DATES COVERED
	June 30, 1995	Final Report, September 1992-March 1995

4. TITLE AND SUBTITLE

Development of a System for Improved Helicopter Blade Tracking - Phase II

5. FUNDING NUMBERS

DAAJ02-93-C-0013

6. AUTHOR(S)

Richard L. Bielawa and Kirk Frederickson

7. PERFORMING ORGANIZATION NAME(S) AND ADDRESS(ES)

Renssalaer Polytechnic Institute
110 8th Street
Troy, New York 12180-3590

8. PERFORMING ORGANIZATION REPORT NUMBER

D-95-1

9. SPONSORING/MONITORING AGENCY NAME(S) AND ADDRESS(ES)

Aviation Applied Technology Directorate
U.S. Army Aviation and Troop Command
Fort Eustis, VA 23604-5577

10. SPONSORING/MONITORING AGENCY REPORT NUMBER

USAATCOM TR 95-D-9

11. SUPPLEMENTARY NOTES

Prepared in cooperation with Sikorsky Aircraft Division, United Technologies Corporation.

12a. DISTRIBUTION/AVAILABILITY STATEMENT

Approved for public release; distribution unlimited.

12b. DISTRIBUTION CODE

13. ABSTRACT *(Maximum 200 words)*

This report presents the results of the Phase II experimental verification portion of a research program in support of the development of a quality control system for obtaining improved helicopter rotor blade tracking. The specific objective of the system is the accurate concurrent measurement of both the first and second mass moments (i.e., the static mass moment and the mass moment of inertia). The results of the Phase I study showed that, subject to the strict maintenance of linearity, the eventual system should be capable of making these measurements with accuracies to within 0.02% of nominal values. This degree of accuracy should result in blade-tracking characteristics superior to what are presently measurable and, hence, obtainable. The planned system would involve a horizontally supported blade configuration using a trapeze-like cradle suspension system. The technical basis of the measurement process involves two operations: first, the accurate measurement of the eigenvalues of the essentially rigid-body dynamic system using appropriate transient time histories. and second, the extraction of the mass moments using the measured eigenvalues, together with other known mechanical properties of the system.

The experimental results of this study were twofold:
1) A series of tests were performed on a prismatic aluminum bar having length and mass characteristics of the same scale as those of a UH-60 Blackhawk helicopter rotor blade, but of as simple enough construction to enable analytical prediction of the mass characteristics, and 2) a second series of tests were similarly performed on a population of actual Blackhawk rotor blades to assess variability in properties and correlation with one/rev vibration characteristics.

14. SUBJECT TERMS	15. NUMBER OF PAGES
Helicopters, Rotor Blades, Blade Tracking	78
	16. PRICE CODE

17. SECURITY CLASSIFICATION OF REPORT	18. SECURITY CLASSIFICATION OF THIS PAGE	19. SECURITY CLASSIFICATION OF ABSTRACT	20. LIMITATION OF ABSTRACT
UNCLASSIFIED	UNCLASSIFIED	UNCLASSIFIED	UNLIMITED

PREFACE

This report presents the results of the Phase II experimental verification portion of a research program in support of the development of a quality control system for obtaining improved helicopter rotor blade tracking. The specific objective of the system was the accurate concurrent measurement of both the first and second mass moments, i.e., the static mass moment and the mass moment of inertia. The results of the Phase I study which was sponsored by Sikorsky Aircraft Division, United Technologies Corporation, showed that, subject to the strict maintenance of linearity, the system should be capable of making these measurements with accuracies to within 0.02% of nominal values. This degree of accuracy should result in blade tracking variations smaller than are presently measureable. The planned system would involve a horizontally supported blade configuration using a trapeze-like cradle suspension system. The technical basis of the measurement process involves two operations: first, the accurate measurement of the eigenvalues of the essentially rigid-body dynamic system using appropriate transient time histories, and second, the extraction of the mass moments using the measured eigenvalues, together with other known mechanical properties of the system.

The experimental results of this study were twofold:

1) A series of tests were performed on a prismatic aluminum bar having length and mass characteristics of the same scale as those of a UH-60 Black Hawk helicopter rotor blade, but of as simple enough construction to enable analytical prediction of the mass characteristics, and
2) a second series of tests were similarly performed on a population of actual Black Hawk rotor blades to assess variability in properties and correlation with one/rev vibration characteristics.

ACKNOWLEDGEMENTS

The Rensselaer Polytechnic Institute (RPI) effort for Phase I of this program was supported by Sikorsky Aircraft Corporation Purchase Order Number S2536210. The RPI effort for Phase II was supported by the U.S. Army Aviation Applied Technology Directorate, ATCOM, Contract DAAJ02-93-C-0013. Sikorsky Aircraft Corporation support for testing of rotor blades at the Sikorsky facility, analysis of data and contributions to the final report were funded by Sikorsky internal funds. Dr. Bielawa completed writing of the final report after assuming a position with the Georgia Institute of Technology, Atlanta, Georgia. Dr. Andrew Lemnios of RPI coordinated completion of final report.

The government projects engineers for this project, in succession, were David Kinney and Edward Austin.

TABLE OF CONTENTS

LIST OF FIGURES

LIST OF TABLES

NOMENCLATURE

$A_0 \ldots A_4$	=	coefficients of the characteristic equation
B_1	=	effective viscous lineal damping at area center of test article. lb_f-sec/ft
B_2	=	effective viscous rotational damping, lb_f-sec-ft
$F_1(t_k)$	=	load in lateral spring no. 1 sampled at the k th instant of time
f	=	frequency, Hz
f_c	=	corner frequency of low-pass filter, Hz.
f_n	=	natural frequency, Hz
f_s	=	sampling frequency in A/D conversion, Hz
g	=	gravitational acceleration, ft/sec^2
H	=	suspension height of cable supporting test cradle, in
$I_{zz_{1B}}$	=	second weight moment of inertia of the test article (metric inertia bar or rotor blade) about the cradle reference point, $1b_f$-ft^2
$I_{zz_{2B}}$	=	second weight moment of inertia of the test article (metric inertia bar or rotor blade) about the test article reference point, $1b_f$-ft^2
$\tilde{I}_{zz_{1C}}$	=	second weight moment of inertia of the cradle assembly with the effective masses of the lateral springs about the cradle reference point, lb_f-ft^2
$I_{zz_{1C}}$	=	second weight moment of inertia of the cradle without the effective masses of the lateral springs about the cradle reference point, lb_f-ft^2
I_b	=	rotor blade second mass moment about articulation hinge, lb_f-sec^2-ft
ΔI_b	=	variational increment (deviation from manufacturing specification) in rotor blade second mass moment, lb_f-sec^2-ft
$\bar{k}$	=	radius of gyration of the combined inertia (test article, cradle and lateral springs) about its center of gravity, nondimensionalized by the length, L
$\bar{k}_w$	=	radius of gyration of a typical support cable about a transverse axis through its mass center, nondimensionalized by the cable length, H
K_1, K_2	=	spring stiffnesses of transverse cradle to floor support springs, lb_f/in
L	=	horizontal distance separating cables at ends of cradle, in
M	=	mass whose inertia characteristics are to be measured, lb_f-sec^2/ft
m_w	=	total mass of the support cables (wires) (4 x mass of one cable), lb_f-sec^2/ft
n	=	number of separate time-history results used, usually eigenvalue sets
N_s	=	number of time-sampled values comprising a time history
R	=	rotor radius, ft
$[R]$	=	characteristic equation partial derivative matrix, multiplies vector of differentials of the eigenvalues
S_b	=	rotor blade first weight mass moment about articulation hinge, lb_f-sec^2
$S_{x_{1C}}$	=	first weight moment of the cradle assembly about the cradle reference point lb_f-ft
$S_{x_{1C}}$	=	first weight moment of the test article about the cradle assembly reference point, lb_f-ft
$S_{x_{2B}}$	=	first weight moment of the test article about the test article reference point, lb_f-ft
$[S]$	=	characteristic equation partial derivative matrix, multiplies vector of

		differentials of the mechanical parameters ($\bar{k}^2$, η, B_1, & B_2)
t	=	time, sec
t_k	=	k th value of sampled time, sec
W	=	transverse spacing of suspension cables, in
W_B	=	measured weight of the test article (metric inertia bar or rotor blade), $1b_f$
W_C	=	measured weight of the cradle assembly (w/o lateral spring weights), $1b_f$
$\tilde{W}_C$	=	weight of the cradle assembly with effective weight of lateral springs included $1b_f$
W_{K_1}, W_{K_2}	=	measured weights of one each of the pairs of K_1 and K_2 springs, respectively, $1b_f$
W_T	=	measured weight of the total mass supported by the support cables i.e., cradle assembly, test article and springs (= gM), $1b_f$
W_w	=	combined measured weight of support cables, $1b_f$
X_{1_a}, X_{1_b}	=	longitudinal forces at corners of the "root" end of the support cradle assembly, $1b_f$
X_{2_a}, X_{2_b}	=	longitudinal forces at corners of the "tip" end of the support cradle assembly, $1b_f$
x_1, x_2	=	longitudinal positions relative to cradle and test article origins [The cradle assembly origin is taken as the no. 1 cable attachment point.], ft
$x_{1_{ref}}$	=	reference point of test article origin relative to the cradle origin, ft
Y_1, Y_2	=	transverse forces at the "root" and "tip" ends, respectively of the support cradle assembly lb_f
$y_1(t), y_2(t)$	=	transverse deflections of the support cradle at the "root" and "tip" ends, respectively, of the support cradle assembly in,
$\hat{y}(t)$	=	transverse deflection of the center of gravity of the support cradle assembly, in
Δz_{tip}	=	blade (tip)_ out-of-track, mm
β	=	blade flapping angle, deg
$\Delta\beta$	=	total blade out-of-track flapping angle, deg
η	=	distance of mass center from "root" end of support cradle, nondimensionized by L
η_B	=	distance of mass center of test article from "root " end of support cradle, nondimensionized by L
$\tilde{\eta}_B$	=	distance of mass center of cradle assembly (with effective lateral spring masses) from "root" end of support cradle, nondimensized by L
ψ	=	yaw angle of support cradle, rad
λ	=	system eigenvalue (= $\sigma + i\omega$), sec^{-1}
σ	=	real part of system eigenvalue, giving stability information, sec^{-1}
ω	=	imaginary part of eigenvalue, giving coupled frequency information, rad/sec
ω_n	=	natural frequency, rad/s
ω_P	=	pendular frequency of a physical pendulum, rad/s
ω_S	=	natural frequency of a spring-mass system (in extentional motion), rad/s
ω_0	=	basic pendular frequency for a point mass, rad/s

Subscripts

$()_1, ()_2$	=	relating to rigid-body oscillatory modes 1 and 2, or to "root"
$()_k$	=	taken at the k th time sampling

Superscripts

$(\overline{\cdots})$	=	nondimensionalization by combinations of L and M or complex conjugate, as appropriate
$(\tilde{\cdots})$	=	Nondimensionalization by H

1.0 INTRODUCTION

1.1 Background

Although all manufacturers of helicopter rotor blades rigorously attempt to make each of their blades identical to every other, the remaining dissimilarities (due to ever-present manufacturing variability) allow sufficient transmission of the "off-integer harmonic" blade root shears and moments to cause vibration problems. These harmonics become increasingly noticeable as means for controlling vibration due to other causes become more effective.

The basic standard procedure used by blade manufacturers is to balance each blade relative to a "master" blade. Thus, each blade is balance measured and adjusted to have the same static balance characteristics as the master blade. Specifically, the *first* mass moment of inertia is measured and brought to a standard value by removing or adding small masses at a "tip box". This procedure, which ignores the possibility of flapping (*second*) mass moment of inertia mismatch, minimizes unbalanced inplane centrifugal forces at once per revolution, as long as the blades are straight out in the unconed position ($\beta_0 = 0$). In flight, however, the coning angle is no longer zero. Putting blades "in-track" with mismatched second mass moments of inertia is normally accomplished by adjusting trim tabs so that aerodynamic force imbalances compensate for the inertial force at one specific flight condition. However, since aerodynamic mismatch changes with flight condition, and with forward speed in particular, blade out-of-track and vibrations will still occur at other parts of the flight envelope. Furthermore, while it can be shown that an in-track condition will minimize inplane unbalanced loads when the blades are coned, it is not at all certain that such an in-tracked condition (with commensurably mismatched aerodynamic and dynamic forces) will minimize the nP vertical blade root shears. In fact, it is possible that, as far as vertical root shears are concerned, the out-of-track condition may even define a reduced nP vibration condition.

Improved tracking methods that are flight-condition insensitive are especially important for today's faster helicopters. Of particular interest is the servicing of two helicopter models forming a major part of the U.S. Army inventory: presently, the UH-60A, Black Hawk, and, in the future, the RAH-66, Comanche. Of these the Black Hawk is currently of principal importance owing to its fleet size and high degree of utilization.

1.2 Research Objectives

The general overall research objective of this program, including all phases, is to develop the technical basis and practicality of, and formulate design specifications for a new automated system for balancing production blades for accurate measurement and control of both first *and* second mass moments of inertia. This general research objective was to be accomplished by meeting the following specific technical objectives:

1) Develop theoretical analyses for relating first and second mass moments of inertia to measured rigid-body (pendular) natural frequencies and other geometrical characteristics for a complete dynamic description of the proposed system and for predicting accuracy limits based on the derived dynamic analysis.

2) Design and fabricate a practical prototype test setup which would be capable of implementing the theoretical development. Included in this test setup would be the identification and acquisition of practical instrumentation for achieving the test objectives.

3) Verify the theoretical development with the test setup and a known prismatic bar inertia. In particular, verify that the experimentally obtained value of inertia for the prismatic bar correlates well with the value determined analytically using standard formulas for the component parts and their combination.

4) Identify the pertinent parameters contributing to system accuracy and find optimal values.

5) Validate the system by applying it to a population of actual helicopter rotor blades. This application should consist of measuring the moments of inertia of the blades and relating the inertias to actual blade tracking characteristics. If a set of poorly tracked blades with commensurately mismatched inertias can be identified, find modifications that match inertias within the set and demonstrate improved tracking with the modifications.

6) Develop an efficient and practical computer-controlled design and dedicated software for an eventual ruggedized system suitable for operation both in an industrial (manufacturing) environment and in service-oriented operations.

Of these technical objectives, Items 1 through 3 have been accomplished. Item 1 was accomplished in Phase I and is described in Reference 1; this item was also addressed further herein. Item 4 was partially addressed in Reference 1. Item 5 was indirectly addressed and only partially accomplished. Item 6 remains to be accomplished.

1.3 Basic Description of the System

1.3.1 Pictorial and General Functional Description of the Mechanical Elements of the System - The ultimate goal of this study was the definition of a system that would be capable of determining blade second mass moment of inertia with sufficient accuracy to reduce significantly the effort currently spent in tracking rotor blades. That is, we desired a superior method of quality control that would enable the manufacture of rotor blades with controlled standardization of second mass moment of inertia. Inherently, a *dynamic* principle must be utilized in the system since the second mass moment of inertia is itself a "dynamics-related" parameter and cannot be measured statically. Specifically, the factors that must be considered in the system are as follows:

1) The dynamic principle to be used must operate at a sufficiently low frequency that the elastic vibrational modes of the rotor blade (or the test structure itself) are not excited.

2) The system must have a high degree of linearity to enable an accurate mathematical simulation of its dynamics.

3) The system should be simple so as to minimize equipment costs and sources of error.

4) The accuracy of the system must be quantifiable.

Various forms of pendular (rigid-body) systems have been used for many years for measuring second mass moments of inertia. Indeed, one approach initially considered was to implement a full-scale version of a pendulum technique used commonly for model rotor blades. In this technique the blade is swung from an initially vertical position about a pivot point as a one-degree-of-freedom physical pendulum. With this technique the mass and mass center are first measured; the pendular frequency

ω_p is then measured, and the second mass moment is then calculated using the simple formula for an undamped physical pendulum, Reference 2.

$$I_b = S_b g/\omega_P^2 \tag{1}$$

Difficulties arise with this method for full scale blades, however, in that (a) it becomes difficult to mount a rotor blade in a vertical position with a sufficiently low friction pivot, (b) the accurate noninvasive measurement of the pendular frequency requires special optical measuring devices or a spring must be added to the dynamics to enable the use of a load cell, (c) the nonexcitation of the elastic natural bending modes is not assured, especially with any inclusion of a spring, and (d) the separate measurement of the first mass moment of inertia is required.

As originally conceived and reported in Reference 1, an alternate system was formulated which overcomes these difficulties. This system is still basically a pendular system, but with the difference that the blade is supported horizontally in a low mass cradle assembly that is confined to move in only two *essentially rigid body* degrees of freedom, as shown in Figure 1.

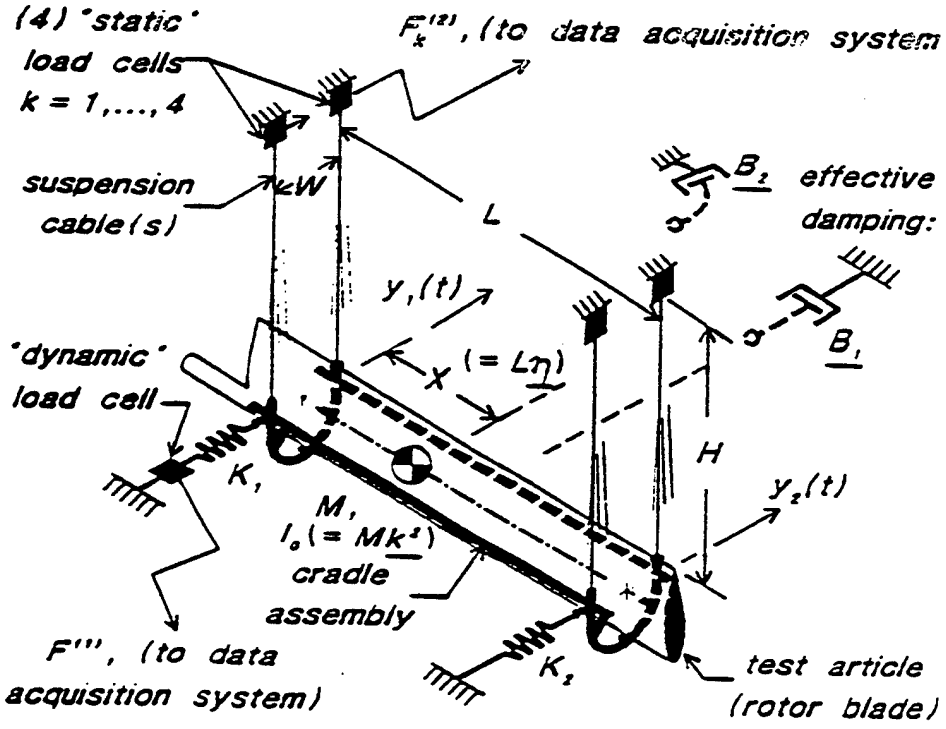

Figure 1. Schematic of blade in devised pendular suspension system.

The above figure defines a simple two-degree-of-freedom system wherein the rigid-body mass, consisting of a cradle and the test article (rotor blade), is suspended by four suspension cables and restrained by the restoring forces of the suspension cables and the two transverse springs, K_1 and K_2. Note that the use of four cables ensures that the rolling degree of freedom has been constrained out of the system. Additionally, two sources of effective damping can be assumed to exist. One effective damper, B_1, resists the translational motion of the mass center $\hat{y}(t)\ [= \frac{1}{2}(y_1(t) + y_2(t))]$, and another, B_2, resists the yawing motion of the combined cradle assembly $\psi(t)$. In the figure the various dimensions (W, L, and H), the combined cradle/test article assembly mass, M, the two spring stiffnesses, K_1 and K_2, and the gravitational constant, g, are all assumed to be known to a sufficiently high degree of accuracy.

The four underlined quantities, $\underline{\bar{k}^2}$, $\underline{\eta}$, $\underline{B_1}$, and $\underline{B_2}$, are unknown and must be determined from the above identified known quantities and the accurately measured damped natural frequencies (eigenvalues) of the system. Since the combined cradle/test article assembly mass, M, is known by measurements of weight, the quantities, η and $\bar{k}^2$, are measures, respectively, of the first and second mass moments of inertia. As originally described in Reference 1, the methodology does not require an independent measurement of the first mass moment of inertia, as the evaluation of this necessary parameter can be one of the principal results. However, as is discussed in a subsequent section, improvements in the accuracy of the results can be achieved if an independent measurement of the first mass moment (as would be provided by current static moment measurement schemes) is used. Thus, Figure 1 shows the inclusion of tension sensitive load cells mounted at the top ends of each of the cables to measure the static loads.

1.3.2 Description of the Required Instrumentation Components - The instrumentation requirements for the system are relatively simple, but care must be taken to insure accuracy. As presently configured, the *static* tensile loads in the cables, which give a measure of test article weight and first mass moment, are to be measured by load cells at the top of the cables where they attach to the upper support frame. The time histories of the motion are to be measured by means of a high-sensitivity load cell attached in series with the K_1 spring.

Figure 2 presents the basic functional components of the total system. Two principle functions are defined: (a) a data acquisition function consisting of sensors to measure the physical cable loads and time histories and support instrumentation controlled by an appropriate data acquisition program, and (b) an extraction function that

first extracts the eigenvalues of the system (complex frequencies) and then extracts the required mechanical properties using a regression analysis. These two separate and sequential computer functions form the basis of two separate programs. Both programs are simple enough to be contained in the same conventional PC-sized computer configured to serve as an instrumentation computer. The figure indicates that the final extracted properties are the test article radius of gyration squared, k^2, the center of gravity location parameter, η, (or alternatively, the gravitational acceleration, g, as is discussed in a subsequent section) and the two equivalent damping values, B_1 and B_2.

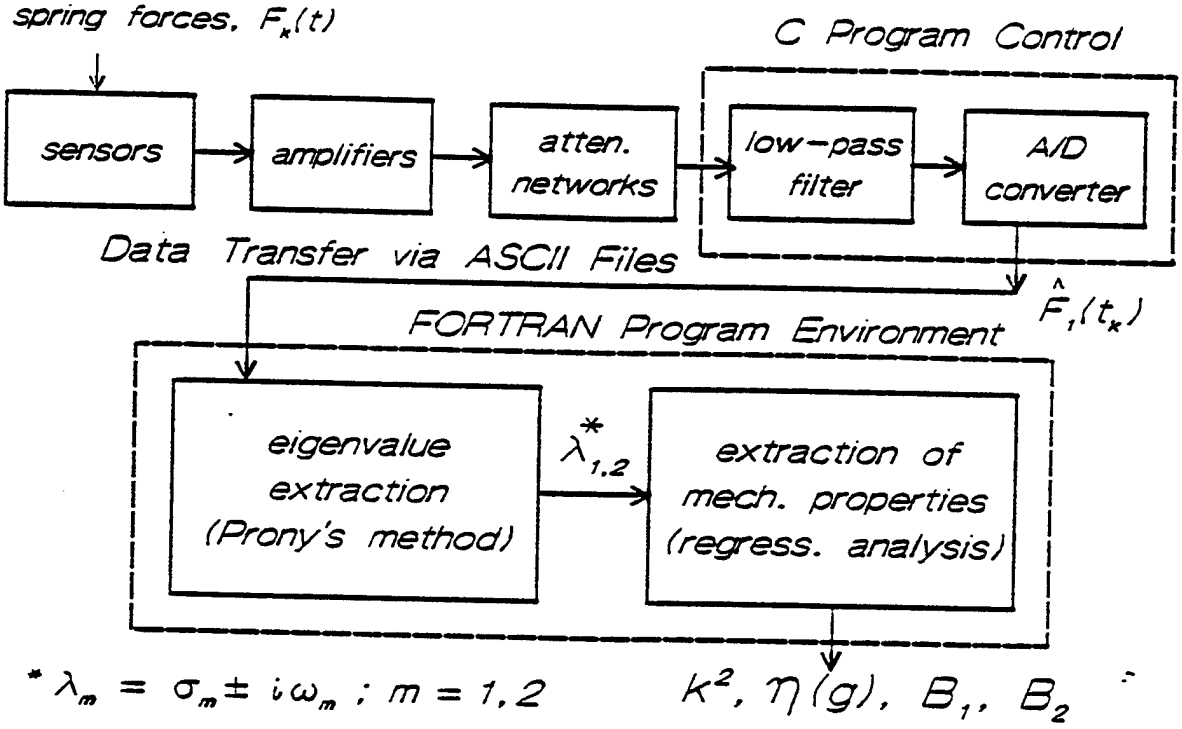

Figure 2. Functional diagram of the Rotor Blade Inertia Measurement System

As the figure shows, the principal part of the operation of the instrumentation subsystem is that component dedicated to reducing the analog time-history transient response of the spring force, $F_1(t)$, to a time series of accurately digitized values at discrete values of time, t_k. This digitization function requires consideration not only of the characteristics of the various components, but also of minimizing the various sources of noise. Additionally, as a simple alternative to extracting the first mass moment within the extraction algorithm, this quantity can be measured directly using the loads in each of the

four cables. Thus, the required components of the instrumentation subsystem are as follows:

1) **A sensitive dynamic load cell** optimized for the low-frequency *dynamic* responses of the spring force, with appropriate amplification and signal conditioning. The emphasis on dynamic response measurement and the need for minimizing noise would suggest the use of a piezo-electric load cell with a battery-powered amplifier.

2) **A low-pass anti-aliasing filter**. Since the analog transient responses are to be digitized, the inaccuracy caused by aliasing effects must be minimized. In the simulations performed and reported in Reference 1, a Butterworth low-pass filter was simulated and optimal results were obtained with a relatively low value of corner frequency. The value of corner frequency for minimum error was found to be near to and actually somewhat below the lower of the two system natural frequencies.

3) **A high resolution A/D converter**. The findings of Reference 1 include simulation results for two available high-resolution A/D converters typically used for chromatography; these converters have resolutions in the range of 20 to 24 bits with relatively low sampling frequencies.

4) **Sensitive load cells for static loads** and appropriate amplification and signal conditioning for accurately measuring the *static* cable loads. For this application the use of strain gage and/or piezoresistive load cells would be favored over the use of piezoelectric types because of the poor DC load measuring characteristics of piezoelectric devices. Additionally, the use of low drift signal conditioning amplifiers would be appropriate.

Figure 2 also shows the two components comprising the computational subsystem. The proper functioning of the computational subsystem depends heavily on three analytical/computational resources:

1) A means for accurately extracting the damped natural frequencies from the digitized time history of the transient motion of the cradle/test article assembly. As with the Phase I development, the use of Prony's method, Reference 3, was retained.

2) A set of dynamic equations that accurately describes the transient motion of the two-degree-of-freedom system. The original equation set is reported in Reference 1. However, during the performance of the Phase II effort some modifications/refinements to these equations were formulated and derived; these upgraded equations are presented in Appendix A.

3) A methodology for extracting the desired dynamic parameters from the measured responses and the known parameters of the system.

Since the dynamic equation set is linear, these equations can be used to relate the eigenvalues, λ (= $\sigma \pm i\omega$), to the physical parameters. Since the dynamic system includes only two degrees of freedom, it is practical to work with the expanded characteristic equation, as the required mathematical relationship linking the dynamical parameters (i.e., the eigenvalues) to the physical parameters. This characteristic equation is of the following form:

$$A_4 \lambda^4 + A_3 \lambda^3 + A_2 \lambda^2 + A_1 \lambda + A_0 = 0 \tag{2}$$

where the coefficients, A_j, are typically algebraic functions of the known parameters, M, H, L, W, ω_0^2, etc., and the unknown parameters, $\bar{k}^2$, η, B_1 and B_2. Note that ω_0 is the simple pendular natural frequency, and $\overline{W}$ is the lateral distance between the cables in direction of the measured transverse motion of the test object nondimensionalized by cable length, L. The actual formulas for the A_j coefficients are given in Appendix A.

The characteristic equation is required as the basis for relating the eigenvalues, as calculated from *measured* transient time histories, to the vector of mechanical properties to be determined. The eigenvalues of the motion of the two-degree-of-freedom system are found from the time series of measured translational motion, accurately digitized values at discrete values of time, t_k, using Prony's method. The second required computational chore is that of extracting the mechanical properties using known physical parameters and the measured eigenvalues; this procedure is described in the following section.

1.3.3 Extraction of Mechanical Properties - The characteristic equation, Equation 2, forms the basis for defining an iterative solution for the required mechanical properties using a regression analysis. Upon taking differentials of the characteristic equation, perturbations in the *four* eigenvalue quantities can be linearly related to perturbations in the *four* required mechanical properties. As developed and reported in Reference 1, the basic set of equations relating perturbations in the eigenvalues to as many perturbations in the selected unknown mechanical parameters is expressable in matrix form:

$$[R]\begin{Bmatrix}\delta\sigma_1\\ \delta\omega_1\\ \delta\sigma_2\\ \delta\omega_2\end{Bmatrix} = [S]\begin{Bmatrix}\delta\bar{k}^2\\ \delta\eta\\ \delta\bar{B}_1\\ \delta\bar{B}_2\end{Bmatrix} \tag{3}$$

where the **R** and **S** matrices are square.

While the details of the differentiations are somewhat tedious, they are nonetheless straightforward. The basic approach is presented in Appendix A and a more thorough treatment is given in Appendix A of Reference 1. In practice, FORTRAN implementations of the evaluations of the elements of the **R** and **S** matrices (using the development of Appendix A) are most efficiently performed using complex arithmetic. This implementation was achieved using program BOOT_K2B.

Equation 3 is used together with an iterative search algorithm formulated using a truncated Taylor's series. Using the straightforward approach formulated in Reference 1, there are four unknowns and four items of required information. Therefore, this truncated Taylor's series takes the following form:

$$\begin{Bmatrix}\bar{k}^2\\ \eta\\ \bar{B}_1\\ \bar{B}_2\end{Bmatrix}_{k+1} = \begin{Bmatrix}\bar{k}^2\\ \eta\\ \bar{B}_1\\ \bar{B}_2\end{Bmatrix} + [U_k]\begin{Bmatrix}\delta\sigma_1\\ \delta\omega_1\\ \delta\sigma_2\\ \delta\omega_2\end{Bmatrix}_k \tag{4}$$

where the $\mathbf{U}_k$ matrix is given by:

$$[U_k] = [S_k]^{-1}[R_k] \tag{5}$$

and where the iteration process is initiated using the results of first solving for $\bar{k}^2$ and η for the *undamped* case (i.e., $\bar{B}_1$ and $\bar{B}_2 = 0$):

$$\begin{Bmatrix} \bar{k}^2 \\ \eta \\ \bar{B}_1 \\ \bar{B}_2 \end{Bmatrix}_0 = \begin{Bmatrix} \bar{k}^2 \\ \eta \\ 0 \\ 0 \end{Bmatrix}_{\substack{\text{undamped} \\ \text{case}}} \tag{6}$$

For the undamped case a direct solution for $\bar{k}^2$ and η is practical using only the frequency parts of the measured eigenvalues, ω_1 and ω_2. Thus, the eigenvalues are approximated by:

$$\lambda_1 \simeq 0 + i\,\omega_1 \tag{7a}$$

$$\lambda_2 \simeq 0 + i\,\omega_2 \tag{7b}$$

As originally developed, the solution for $\bar{k}^2$ and η is accomplished iteratively by means of various algebraic manipulations of Equation 3. The iterative process is started using the above eigenvalue approximations (Equations 7a and 7b). After $\bar{B}_1$ and $\bar{B}_2$ are set to zero, two equations are obtained each defining the characteristic equation for one of the frequencies. Then, $\bar{k}^2$ is isolated using the difference of the two equations, and eliminated by substitution into one of the characteristic equations. As is given in more detail in Reference 1, this operation results in equations for η and $\bar{k}^2$. Note that the use of the undamped characteristic equation provides the basis for starting the iterative solution for the required mechanical properties using the full characteristic equation for damped motion. The iteration is continued until the differences between the four measured eigenvalue components and those resulting from the last iterated values of the mechanical properties are small relative to some arbitrarily selected small number.

As is described in more detail in Section 1.4.3, and in Appendix A, the solution algorithm strategy was modified to account for the fact that η was determined using measured cable loads. With η regarded as a "known" parameter, the solution scheme had the form of having only *three* unknowns to be determined using *four* available eigenvalue component measurements.

1.4 Phase II Technical Approach

1.4.1 General Considerations - Since first and second mass moments of inertia are essentially rigid-body mass quantities, measurement of these quantities must be accomplished in a controlled environment with the rigid-body frequencies well separated

from any elastic modes of vibration. As is described in considerable detail in Reference 1, the use of a pendular, gravity-driven principle together with extremely accurate measurements of the ensuing pendular motion forms the basis of the development. The system should incorporate a computer-driven subsystem with which rigid-body vibrational motion of the blade can be measured with extreme accuracy, filtered, digitized, and then reduced to a time-series stream of displacement values. From these data the natural frequencies of pendular motion can be subsequently extracted using appropriate digital signal processing algorithms. Using separate measurements of the blade mass and other geometric information, the measure natural frequencies of motion can then be used to calculate the first and second mass moments of inertia. Eventually, the final production version of the system would be computer-controlled to provide an automated test procedure.

This final version of the system could be developed to provide digital read-outs of incremental weights to be put both at the "tip box" and at some blade inboard attachment fitting, thereby matching both the first and second mass moments of inertia to production-specified values.

1.4.2 Practical Measurement Considerations - One of the findings of the Phase I work was that the accuracy of the measurements was sensitive to errors in the measurement of the mechanical parameters assumed to be "known". These parameters included the basic dimensions L and H, the spring rates of the two springs K_1 and K_2, and the local value of gravitational acceleration g. Consequently, efforts were made to measure these critical parameters with the precision afforded by a laser-based measurement system. Separate accurate measurements of the spring rates and the gravitational acceleration would have required the use of a gravitometer, which was not available and eventually deemed to be an impractical requirement for the system. Consequently, the equations were recast to minimize the impact of the inaccuracy in the gravitational acceleration constant. What eventually emerged was a reformulation of the dynamics in which only accurate measurement of the *product* of the spring rates with g was required. Using the basic measurement equipment and data reduction tools already required for the inertia rig itself, this product could be measured with sufficient accuracy.

1.4.3 Modifications to the Original Theoretical Development - The important feature of Equation 3 is that it represents a functional relationship between four measurable quantities *in as many* unknown, required quantities. Thus, one problem that arises when

an alternate source of c.g. location information is used (i.e., the cable tension measurements via the static load cells) the equation set becomes over-specified. That is, there are now only three unknown quantities to be determined using four measurement quantities.

The initial approach to this dilemma was to make the gravitational acceleration, g, be the unknown fourth quantity. Reference 4 gives 32.1740 ft/s^2 as a value of g at sea level and a latitude of 45 deg. along with a table of variations for other latitudes. However, results from Reference 1 indicated that inaccuracies or variations in the effective value of g, as would occur due to tidal effects, could have a significant effect on the accuracy of the algorithm used. Efforts to acquire an accurate measurement of the local gravitational constant g, however, were abandoned as being impractical. Instead, the equations of motions were rewritten so as to make the quantity g/H be one of the parameters to be solved for in the regression analysis, instead of the c.g. position η, which is now measured directly using the static load cells. Note that H is the effective length of the cables. This redevelopment solved the one problem of not knowing g to high accuracy *a priori*, and a second problem of no longer requiring accurate knowledge of the lengths of the support wires. Although the lengths of the cables were measured with a laser measuring system, the installation of the cables produced many kinks that would slightly affect their effective lengths. Furthermore, adjustments had to be made to the cable lengths to insure that the support cradle was level and not twisted. Thus, by rewriting the equations of motion so that g and H appear together as a single unknown parameter (g/H), the two problems appeared to have been successfully resolved. Another perceived virtue of this approach was that it would provide a convenient "goodness" number for evaluating the accuracy of the extraction algorithm. The actual implementation for this approach was to select the square of the simple pendulum frequency, $\omega_0^2 (= g/H)$, as the fourth unknown quantity and then compare its computed value to the known value, as determined approximately using the known cable length, H, and an approximate value of g. However, this approach proved less than satisfactory in that the resulting algorithm often gave unrealistic variations in ω_0^2, and even at times, negative values although the values of $\bar{k}^2$ were reasonable.

Of all the other schemes investigated, the one that gave the most consistent results was to use a pseudo-inverse approach. In this approach the number of unknown parameters is again set at three (i.e., $\bar{k}^2, \bar{B}_1$, *and* $\bar{B}_2$) and it is further assumed that ω_1 is principally the translational mode frequency ($\approx \omega_0$) and dominated by g, whereas ω_2 is principally the yawing motion mode frequency and dominated by the spring stiffnesses

and the inertia, $ML^2\bar{k}^2$. In a like manner the vector of eigenvalue quantities used for the regression analysis was also set at three (i.e., σ_1, σ_2, and ω_2) Thus Equation 3 was rewritten as:

$$[P]\begin{Bmatrix}\delta\sigma_1\\ \delta\sigma_2\\ \delta\omega_2\end{Bmatrix} = [Q]\begin{Bmatrix}\delta\bar{k}^2\\ \delta\bar{B}_1\\ \delta\bar{B}_2\end{Bmatrix} \tag{8}$$

where the matrices **P** and **Q** are each 4 x 3 matrices and are respectively formed from the **R** and **S** matrices by deleting the second columns of **R** and **S**. The iterative search algorithm resulting from this approach follows by taking the pseudo-inverse of the **Q** matrix:

$$\begin{Bmatrix}\bar{k}^2\\ \bar{B}_1\\ \bar{B}_2\end{Bmatrix}_{k+1} = \begin{Bmatrix}\bar{k}^2\\ \bar{B}_1\\ \bar{B}_2\end{Bmatrix}_{k} + [\hat{U}_k]\begin{Bmatrix}\delta\sigma_1\\ \delta\sigma_2\\ \delta\omega_2\end{Bmatrix}_{k} \tag{9}$$

where the $\bar{U}_k$ matrix in this case is given by:

$$[\hat{U}_k] = [[Q_k]^T[Q_k]^{-1}[Q_k]^T[R_k] \tag{10}$$

This algorithm then retains the benefits of elimination of η as a search variable, along with the desensitizing of the algorithm from variability in g and H. Generally, this algorithm proved to give the most consistent results and was adopted for the remainder of the study.

2.0 EXPERIMENTAL SETUPS

2.1 RPI Test Site

2.1.1 Support Tower - The test facility consisted principally of an A-frame tower with implementations of the basic features identified in Figure 1. An appropriate site was designated for the facility in the RPI CII high bay area and modifications were performed to the site for installation of the facility. As shown in Figures 3a and 3b, the facility stood to a height of 23.5 ft and thereby "fit", but it still required anchor points and a partial disabling of the overhead crane for installation. Modifications to the CII high bay area consisted of the installation of four floor anchor points and two ceiling support points (for the erection cable pulley blocks). The topmost metal frame and various other steel bracing parts were fabricated by the RPI Academic Shops. The remainder of the tower was fabricated from common lumber. Prior to final assembly the support structure was partially assembled in modules, awaiting the precise measurement of the distance separating the cable attachment points on the steel frame, incorporation of the load cells, the precise measurement of the support wire lengths, and the installation of the support wires.

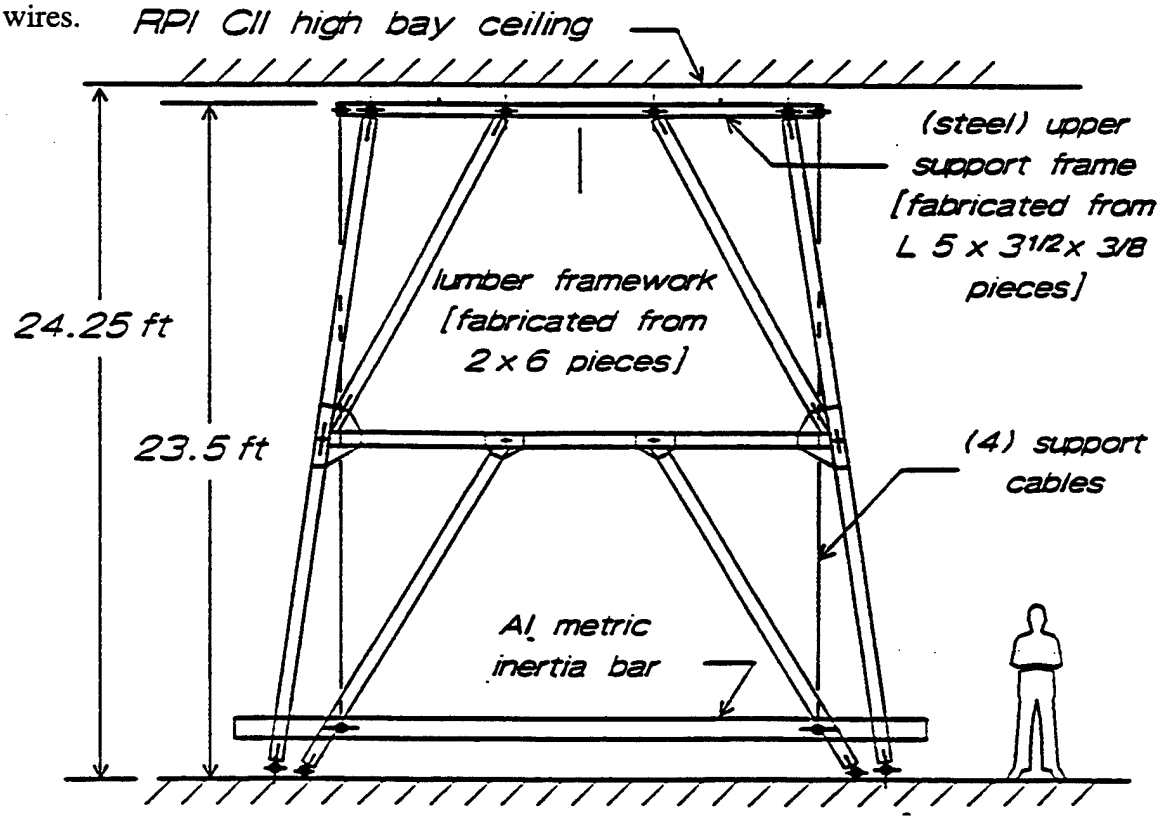

Figure 3a. Pictorial front view of tower assembly with metric inertia bar

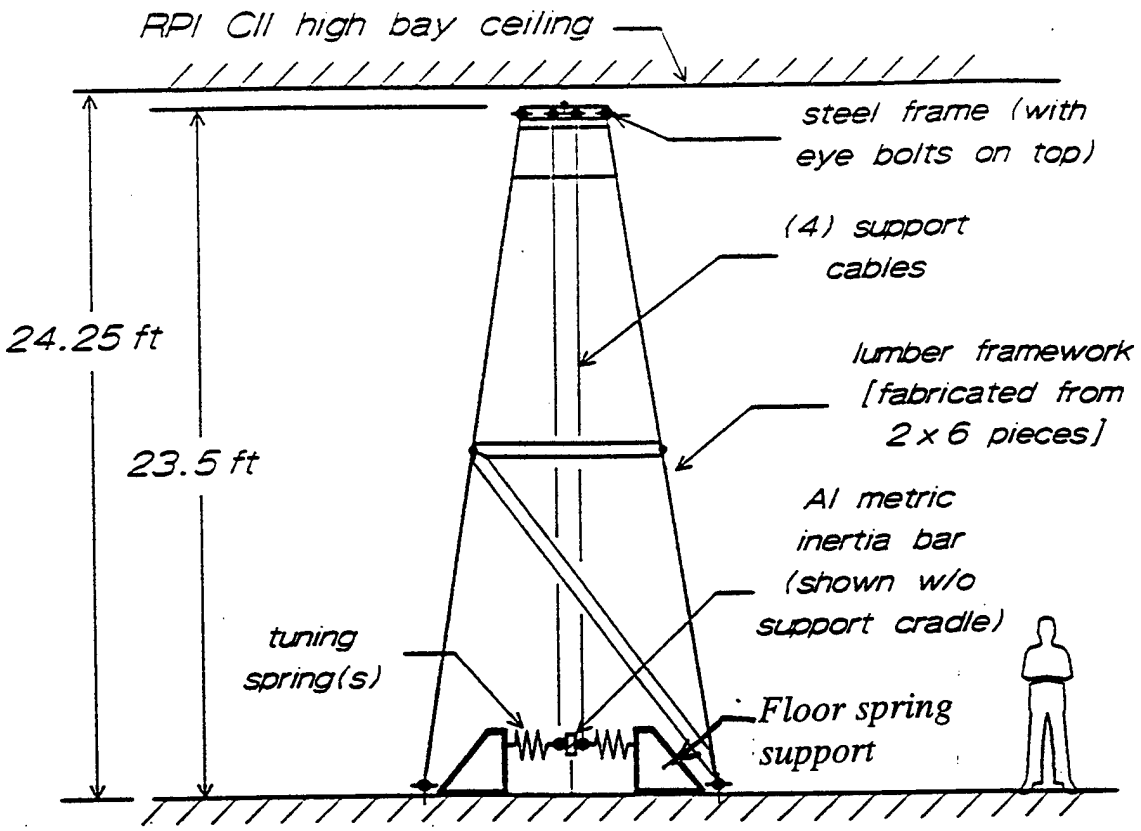

Figure 3b. Pictorial side view of tower assembly with metric inertia bar

Initial assembly and erection of the A-frame consisted of the assembly of structural modules that could be easily bolted together. However, before final assembly could be made, accurate measurements were made of critical dimensions on the top support frame, and the strain gage support wire load cells were calibrated and installed (attached to the top ends of the support cables). The already assembled modules were then connected and final erection of the A-frame was accomplished using winches attached to the base of two of the tower corner posts with cables attached to the tower upper support frame and strung through pulleys attached to the ceiling of the CII high-bay test area. The final erection of the A-frame support structure is shown in Figure 4. The structure was found to be quite robust, with all natural frequencies well above the low frequency (~ 1 Hz) range expected for the actual tests.

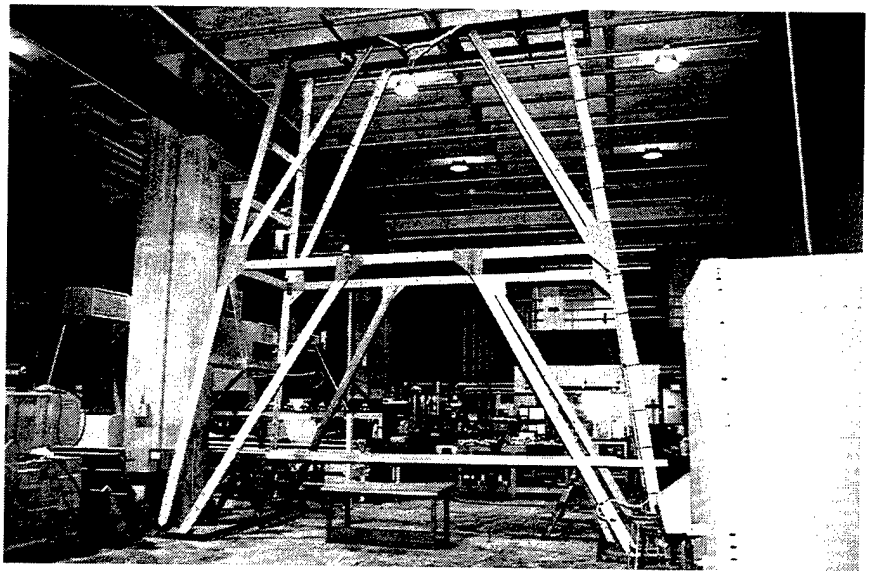

Figure 4. The A-frame support structure erected in the RPI CII high-bay test area

2.1.2 Ancillary Equipment - In addition to the basic A-frame tower and the support cradle, the test facility required four support cables and two floor spring-support and locking frames for attachment of the springs and attached dynamic load cell to the cradle assembly, and for locking the cradle in a secure position. The support cables were fabricated from 1/8 in. diameter (solid) stainless steel cable stock. The cables were cut to a specified length of approximately 20 ft, and threaded with right- and left-handed threads at opposite ends along with portions of brass hex stock at each end for length adjustments. The threaded ends and fittings were used for attaching rod-end bearings to each end of the cables. These bearings connected to eight aluminum clevises. Of the eight clevises, four were required for attaching the rod-end bearings to the static load cells (and thence to the upper support frame) and four for attaching the bearings to the support cradle at the bottom. These clevises were installed after calibration of the load cells and the dimensional measurement of the support wires.

The floor spring-support and locking frames were fabricated from steel angle stock. Attachment of the connecting springs was made with simple eye bolts fastened to the floor frames and to the support cradle with spring attachment posts fastened to the keel of the support cradle. Locking of the cradle was essential for stabilizing the support cradle as well as protecting the support cables and lateral springs while positioning the metric

inertia bar or a Black Hawk rotor blade in the cradle. The method of locking was the use of four (threaded) bolts with attached knobs that mated with threaded nuts welded to the floor spring-support and locking frames. The threaded bolts also served as amplitude limiters when disengaged and partially unscrewed from the support cradle. Future operational installations would require a more compact and quickly activated locking mechanism.

2.1.3 Measurement of Critical Dimensions - Based on the findings of Reference 1, the accuracy of the results were expected to be sensitive to accurate measurements of the horizontal spacing of the support cables, L, and the length of the cables, H. The top support frame was fabricated as a large weldment from structural steel angle bars. Due to the large dimensions involved, fabrication had to rely on simple tape measurements of the support cable attachment bolt holes. Also, the support cables were fabricated with adjustment threads so that the effective lengths of the cables could be varied to achieve uniformity. In addition to the components of the support assembly, the metric inertia bar itself had to be accurately measured to achieve an accurate analytical value for its inertia. Although fabrication of the metric inertia bar was kept simple, it required several repositionings in the milling operation, so that accurate vernier positioning of the mill table was compromised. Thus, in all these cases, measurement of the critical lengths was beyond the scope of available shop measurement resources.

Arrangements were subsequently made with shop personnel at the U.S. Army Watervliet Arsenal for use of their laser-based dimensional measuring system for accurate measurement of all these critical rig and metric inertia bar dimensions. The basic operation of this equipment required the use of a retro-reflector that was manually moved the distance to be measured. It operates on the principle of counting interference fringes, as a direct measure of distance. Use of this equipment required a horizontal placement of the parts and the use of other special jigs for establishing measurement datum surfaces. This scheme required the fabrication of a special (but simple) jig for close parallel positioning and concurrent loading of all the wires, and precision bolts for the steel support frame. Figures 5 and 6 show this equipment being used for measurements of the hole spacing and the length of the metric inertia bar.

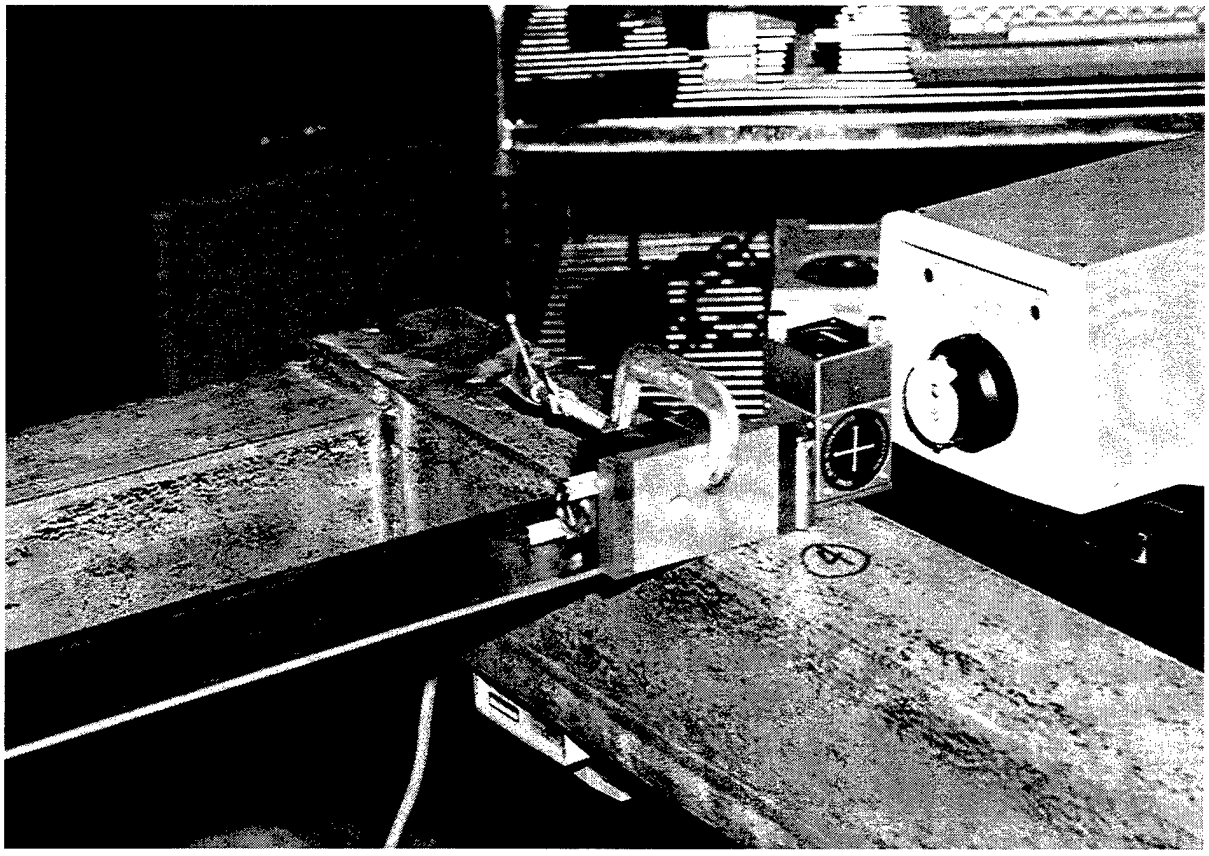

Figure 5. Distance measuring equipment being used to measure support bolt hole spacing on the upper support frame

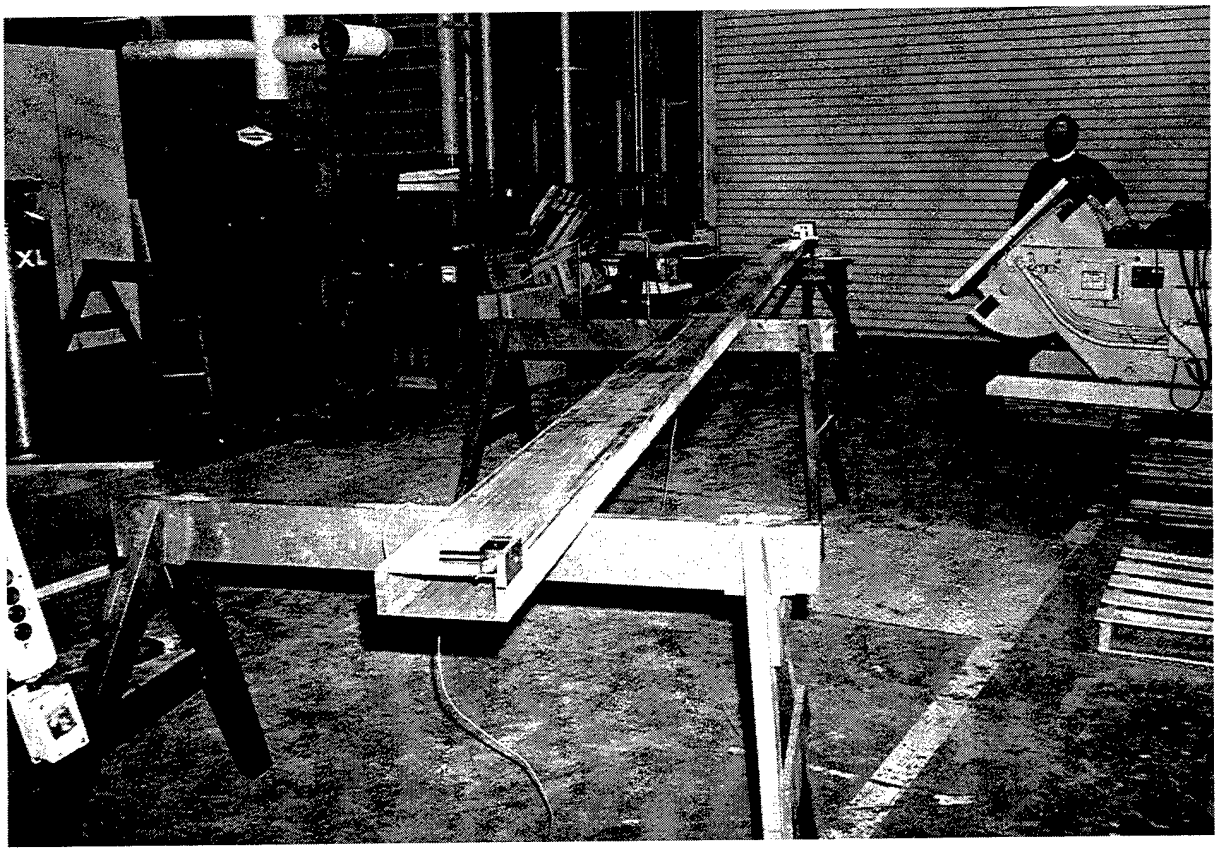

Figure 6. Distance measuring equipment being used to measure length of the metric inertia bar

2.2 Cradle Assembly

The support cradle serves to provide a rigid connection between the test article (metric inertia or an actual rotor blade) and the support cables. As such it needs to be light-weight, stiff, and with a wrap-around geometry to accommodate the test article. The design selected consisted of an aluminum square tube serving as a keel and aluminum angle bars serving as the side rails, and five upside-down, omega-shaped frames, fabricated from 1 in. thick sheet phenolic, equally positioned along the length of the cradle. In addition, tubular stiffening struts were used for attaching the keel to the side rails; these struts greatly increased the rigidity. Also, lightening holes were drilled and reamed in the aluminum keel and side rails to further decrease the weight (and inertia) of the support cradle. The support cradle also had a positioning bar attached to one end to facilitate consistent lengthwise positioning of all test articles in the cradle. Figure 7 presents a view of some of these support cradle features when the rig was installed in the Sikorsky plant.

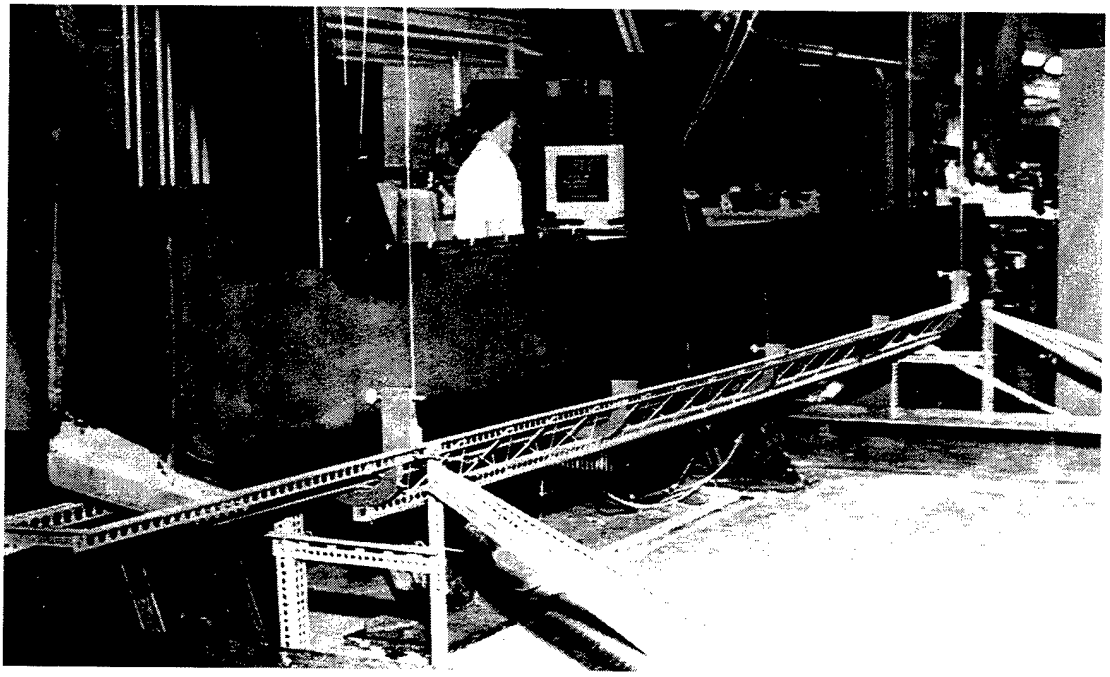

Figure 7. View of Black Hawk rotor blade installed in support cradle, showing floor spring-support and locking frames

For tests with the metric inertia bar at RPI a suitable roller mechanism system was fabricated as a means for providing a practical horizontal means of entry for the metric inertia bar and, later the actual rotor blades (not shown in Figure 7). As is described in more detail in a subsequent section, these rollers were removed for the tests at the Sikorsky plant. Figure 7, furthermore, shows that the end phenolic frames were higher than the inner three frames. The end frames each had five roller mechanisms, two on each side and one on the bottom, for direct support of the test article. The inner three frames only had three roller mechanisms each, again with one at the bottom for direct support of the test article. The tubular stiffening members were fabricated from 6061-T6 aluminum and hence, after being cut to side had to be annealed prior to final fabrication which included end crimping, bending and hole drilling. This annealing was performed at RPI at the Material Research Center. After this fabrication was completed the struts were then brought back to full T6 heat treatment strength. Before the cradle underwent final assembly, the various components were carefully weighed and distances measured. Additionally, a selection of precision springs with sets of selected spring rates was acquired; the nominal values of spring rate selected were 1.4, 4.2, 11.3, and 15.2 lb/in, respectively. Once the support cradle assembly was completed, attachments to the support cables and the lateral springs were installed and the cradle was installed in the facility.

2.3 Metric Inertia Bar

The metric inertia bar was designed to consist of two aluminum channels bolted together to form a hollow rectangular tube, Figure 8. Its length and width were

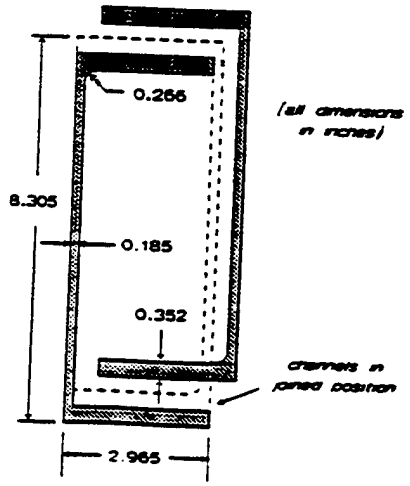

Figure 8. Cross section of metric inertia bar, showing interlocking channel construction

selected to be reasonably compatible with the weight and geometry of the Black Hawk rotor blade; final design for the inertia bar resulted in a 281.965 in. length, as measured using the laser-based measurement system, and a width of 2.965 in. The two channels were stock aluminum 3 in x 8 in parts, as ordered, but the resulting dimensions were closer to 2.965 x 7.953, as delivered. As the figure shows, some machining was required to enable the two channels to be joined. In addition, 20 holes were required on each channel. Ten were drilled, reamed and counterbored in one flange, and ten drilled and threaded with 6-32 thread on the other flange for joining with the other channel. Because of the long length of the inertia bar, the machining had to be done in sections, with the bar being repositioned several times. Consequently, there were some minor variations in the dimensions, and therefore, the dimensions given in Figure 8 are averaged values. Based on the measurements of the cross-sectional area given in Figure 8, the following (estimated) properties for the bar were established:

Table 1. Analytically estimated properties of the metric inertia bar

Property	Value	Units
weight	87.75	lb
S_{x1}	26,468.3	lb-in
$x_{c.g.}$.	140.98	in
I_{zz1}	4,975,600.	lb-in^2
I_{zz_0}	1,244,130.	lb-in^2
$k^2_{zz_1}$	26,501.7	in^2
$k^2_{zz_0}$	6,626.6	in^2
k_{zz_1}	162.79	in
k_{zz_0}	81.404	in
$\left(k_{zz_o}/L\right)^2$ $\left(=\bar{k}^2\right)$	0.1798	ND

2.4 Instrumentation

2.4.1 Sensors and Support Equipment - In addition to the motion measuring piezoelectric load cell and associated battery-powered instrumentation module, four (4) conventional, precision Wheatstone bridge type load cells were acquired to measure the static loads in each of the support cables. This additional instrumentation was necessary to provide a means for measuring blade weight, a redundant source of first weight moment, and the tension in the cables, enabling eventual determination of the change in cable length due to elasticity. The acquired load cells used an existing instrumentation module system already available to the principal investigator at RPI.

The outputs from the all instrumentation modules were scaled to give full range analog outputs of from zero to 2 volts using appropriate attenuation networks prior to input either to the digitally programmable low-pass filter (dynamic load cell signal) or directly to the A/D converter (static load cell signals). The low-pass filter had a tuning range of from 0.1 to 25.6 HZ in steps of 0.1 HZ, tunable by appropriate logic settings on (8) bit selection pins.

All analog signals were digitized using a high-resolution A/D converter which was developed primarily for chromatography applications as a PC AT compatible plug-in board. It was configured using C-language coding. Characteristics of this card that were found to be useful to this study were:

1) Variable (arbitrary) resolution from 18 to 24 bits. However, variability in resolution came at the expense of reduced throughput.

2) Autocalibration ability to restore the board to factory-shipped accuracy at any time, automatically.

3) Use of high-level language (C) to configure the board, using a built-in microprocessor. The resulting command-driven operation allowed data-taking to be accomplished using a user-developed program with data logging to ASCII DOS files.

4) Available digital I/O allowed the board to set bits on a digitally programmable low-pass filter in response to arbitrary user selection of corner frequency.

2.4.2 Data Acquisition System - All features required to acquire the data, except for the sensors, were incorporated into a single conventional rack mount system as shown in Figure 9:

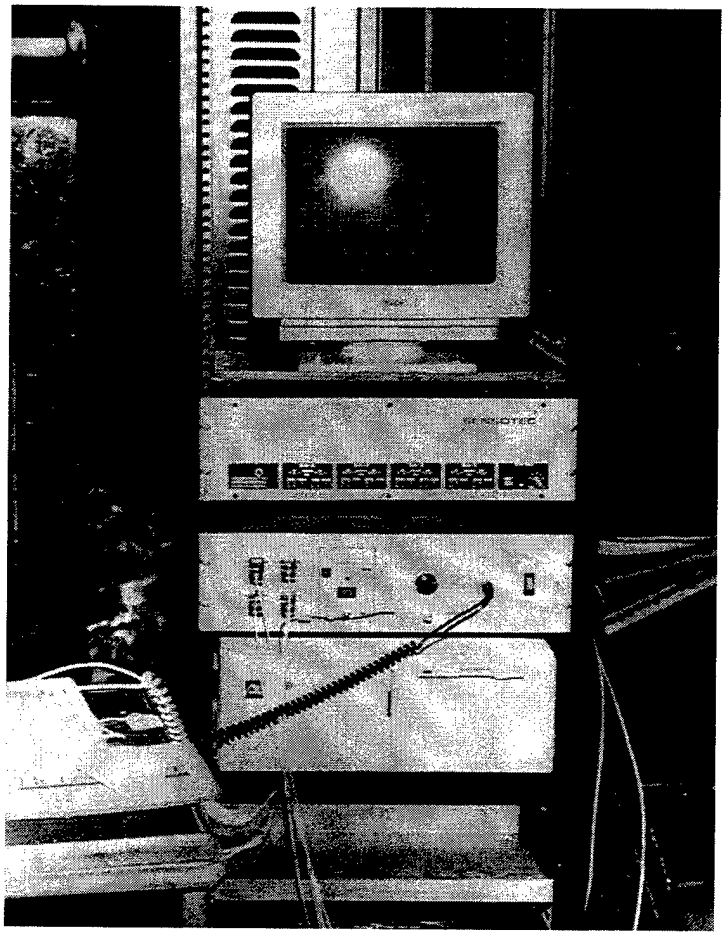

Figure 9. Data acquisition system

This system consisted of three main modules; as seen in Figure 9 from top to bottom below the CRT monitor: (a) a load cell instrumentation amplifier unit, b) the system instrumentation control module, and c) an instrumentation computer.

The system instrumentation control module was a customized chassis that performed the following functions:

1) Provided excitation power for the static load cells from the instrumentation module, power for a circuit board controlling the operation of the programmable filter and related circuits using an included 5 volt power amplifier, and power for the dynamic load cell from the internally battery-powered instrumentation module which was also installed in the front panel of the system instrumentation control module.

2) Provided complete I/O connections for all load cell cables.

3) Provided switch selection of which of the five load cell outputs was to be input to the filter and digitized.

4) Housed the digitally programmable low-pass filter and circuitry for driving the bit values on the pins of the filter. It also presented a panel verification display (with an LED array) of what the actual logic settings were on the filter corner frequency programming pins. This display was then available for comparison with and confirmation of the pin logic settings called for by the data acquisition program, and displayed by the program as an output to the CRT monitor screen).

5) Housed the attenuation circuitry for both types of load cells for achieving the proper input voltage range to the A/D converter. While a simple voltage divider circuit was acceptable for the "static" (Wheatstone bridge type) load cell instrumentation, a high input impedance voltage follower operational amplifier circuit was required for the "dynamic" piezoelectric- type load cell instrumentation.

6) Provided a panel-mounted connection for a hand-held digitization trigger switch for activating the A/D converter.

Calibrations made of the support-wire (static) load cells showed that RMS error bands of approximately 20 μV (relative to the 0 to 2 V digitization range) were obtainable with the instrumentation system. For these load cells the low-pass filter was not used,

however, since the filter imposed a low offset DC voltage and it was found that the error band was less without the filter than with it. The offset voltage was not a factor with the dynamic load cell data acquisition and for these cases the filter was used, as specified.

The instrumentation computer was used for actual data acquisition and for subsequent data reduction. Besides providing a suitable platform for the A/D converter, the computer served as a resource for collecting the acquired data on ASCII data files using standard micro diskettes. In the conceptual design for this system it was envisioned that the eventual production version would be substantially automated and the PC implementation would be the basis for this automation.

2.5 Weight Measurements

All small part components of the rig were weighed using conventional electronic digital laboratory scales which had been calibrated using a set of standard laboratory weights. It was originally intended that the inertia of the support cradle could be calculated using established formulas for moments of inertia for basic conventional shaped solids. This approach was subsequently abandoned as being too time-consuming and prone to potential inaccuracies due to errors either in analysis and/or FORTRAN implementation. The weight measurements were used, however, as a standard in establishing correct measurements of support cradle weight using the static load measuring load cells. It was eventually assumed that the best way of treating the inertia of the support cradle was to test it using the basic measurement technique directly.

2.6 Measurements of Spring Rates

Initially, four sets of springs (five springs each) with nominal spring rates of 1.4, 4.2, 11.3, and 15.2 lbf/in, respectively, were acquired. These springs were respectively denoted the "A", "B", "C" and "D" springs. The "C" springs were found to have insufficient extensibility and were discarded from the tests. Furthermore, in tests of the support cradle alone, the "A" springs were found to be unacceptable because the resulting rigid-body natural frequencies coupled with the lateral "vibrating string" modes of the support cables. These additional responses constituted a significant amount of noise that was unacceptable. Consequently, a set of even softer "E" springs with a spring rate of approximately 0.51 lbf/in was acquired. The resulting rigid-body natural frequencies were significantly removed from the vibrating string modes of the support cables, but the lower spring rate resulted in a reduced signal level from the dynamic load force

transducer. With this reduced signal level came a commensurate drop in signal to noise ratio and coherence from the frequency extraction algorithm.

Spring rates of the various springs were measured using single-degree-of-freedom (extensional) dynamic oscillation tests with variations in attached mass. These tests consisted of first recording the time histories of the damped, single-degree-of-freedom responses using the same instrumentation as used in the main tests, and then applying Prony's method to extract the single damped frequency values. See Section A.1 of Appendix A for a more detailed description of this application. The actual tests with the incremental masses required care is insuring that the resulting oscillations were purely extensional with no pendular motion. For some combinations of spring and mass it was found to be too difficult to avoid the nonlinear coupling with the pendular motion and results with these combinations were discarded. Figure 10 shows the simple set-up used for measuring the time history responses of the spring-mass system including the test spring:

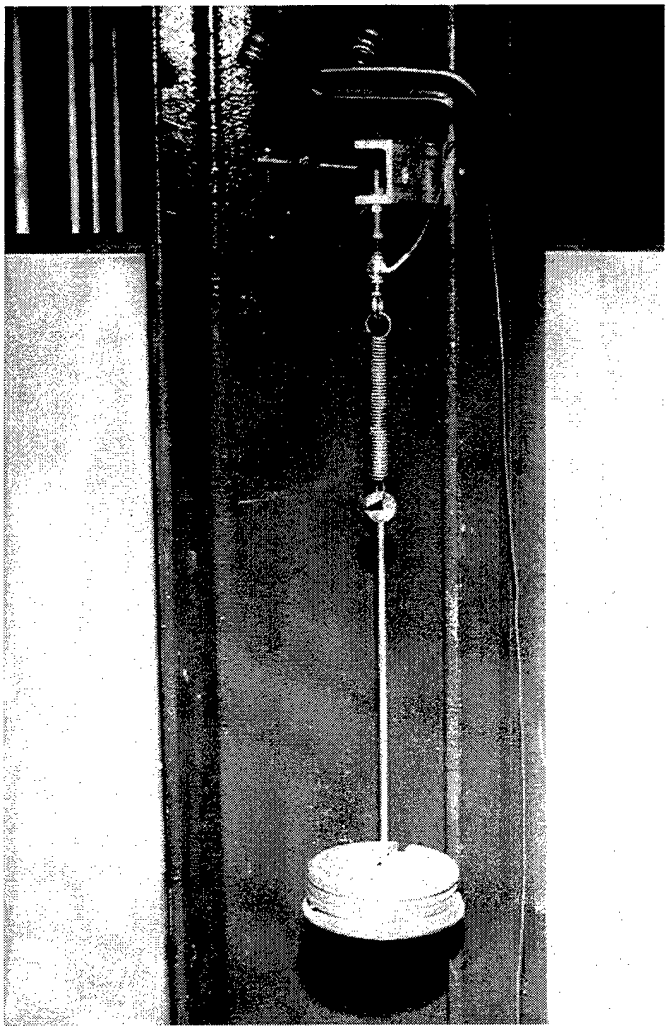

Figure 10. Test set up for measuring spring rates of lateral support springs

A summary or the spring properties of the springs tested is presented in Table 2.

Table 2. Measured spring properties

Spring ID	gK (lb_w/s^2)	W_K (lb_w)
A-1	574.87	0.0839
A-2	573.59	0.0838
A-3	576.55	0.0838
A-4	573.03	0.0838
A-5	574.01	0.0838
B-1	1584.09	0.0287
B-2	1585.78	0.0288
B-3	1598.28	0.0288
B-4	1597.00	0.0288
B-5	1580.98	0.0287
C-1,..,5	*(not used)*	
D-1	4282.91	0.0072
D-2	4264.44	0.0072
D-3	4214.82	0.0072
D-4	4271.66	0.0072
D-5	4232.81	0.0072
E-1	210.61	0.0080
E-2	207.24	0.0080
E-3	207.40	0.0078
E-4	207.05	0.0079

2.7 Sikorsky Plant Test Site

2.7.1 Installation of the Test Rig - After tests at the RPI test site were completed, the upper support frame, the ground spring support and locking frames, support cables, inertia bar and all test instrumentation were transferred to the Sikorsky plant for further testing. The wooden parts of the support tower used at RPI were not transferred. The upper cable support frame was clamped to the overhead structure in the Airframe Static Test Area of the Sikorsky Development Center high bay, as shown in Figure11.

Figure 11. View of top support frame installed in Sikorsky Experimental High Bay Area

This arrangement resulted in the cradle being approximately one foot higher than it was in the RPI facility. The floor spring support and locking frames were accordingly raised to the proper position with respect to the cradle using portable jacks. During testing of the Black Hawk blades, the blades awaiting testing were kept in a blade handing dolly adjacent to the cradle. Each blade to be tested was first lifted with an overhead crane, one support cable was disconnected from the cradle, and the blade then moved into position. The cable was then reconnected and the blade was lowered into the cradle. This procedure was reversed for removing the blade from the cradle. The ambient conditions in the test area were normal room temperature with generally little air movement. The instrumentation, including static load cells and amplifiers, was warmed up for at least one hour prior to testing.

2.7.2 Modifications to the Support Cradle - The cradle was originally designed to hold both the metric inertia bar and the Black Hawk rotor blades. It was simply configured with rollers at the bottom and inner two sides of each of the five U-shaped phenolic cradle frames so that either the metric inertia bar or the Black Hawk blades could be inserted into the cradle horizontally from one end of the cradle. As is described in a earlier section,

frames to assist in inserting and removing of the metric inertia bar or Black Hawk blades. In the case of the metric inertia bar, the test article was regular with no twist. However, the roller installation perfected for the metric inertia bar proved to be impractical for the Black Hawk blades. The rollers were too narrow, especially at the bottoms of the phenolic frames, to accommodate the sharp leading edges of the significantly twisted rotor blades.

It was originally intended that the rollers would be repositioned and reattached to locations on the phenolic frames which would then accommodate the Black Hawk rotor blades. However, to save time the rollers were instead removed and small hard rubber pads were bonded to the bottom center of each of the U-shaped phenolic cradle frames. The leading edges of the test blades then rested on these rubber pads. Each of the frames was then drilled to accept four threaded rods with plastic swivel pads to hold the blade in position. The blades were positioned in the cradle with the chordline vertical at the 75% span position. The swivel pads were adjusted to contact the airfoil at each location and the pads on the *lower* surface of the blade were never moved. The swivel pads on the *upper* surface were loosened to install the blade in the cradle and then tightened to hold the blade securely in place for testing. The blade weight and first and second mass moments of the modified empty support cradle were remeasured using the same methodology that was used for the cradle with test article. These characteristics were then used as the new "tare values" for subsequent tests (see Section A.3 of Appendix A).

2.7.3 Blade Positioning Fixture - It was intended that the blades be entered into the support cradle horizontally at one end and longitudinally positioned using a stop bracket for the blade tip, as was successfully done with the metric inertia bar. The selection of the blade tip was an impractical choice. however, since the Black Hawk blade tips have substantial sweep and droop and, hence, would not actually contact the stop bracket. Additionally, the blades are manufactured for quality control with all dimensions relative to the blade root. Thus, even for a well-matched set of blades, the radii of the blades, as defined by the outer blade tip caps, might well have deviations.

To assure that each blade was in the same spanwise position when entered into the cradle, a fixture for attaching to the blade root was built. As shown in Figure 12, this fixture consisted of two threaded rods securely attached at one end to the cradle and at the end to fittings that accept a blade retention pin installed in the blade cuff. The combined weight of the rods, attachment hardware and fittings was 0.81 lb each and the weight of the typical retention pin was 2.16 lb. For test purposes, the mass and inertia of this

assembly was included in the blade test measurement results. Tests were conducted with and without this fixture to measure its mass properties. However, the results were not consistent enough to subtract from the blade data. If follow-on testing is done, this fixture could be used to position the blades, and then be removed when the blade mass properties are measured.

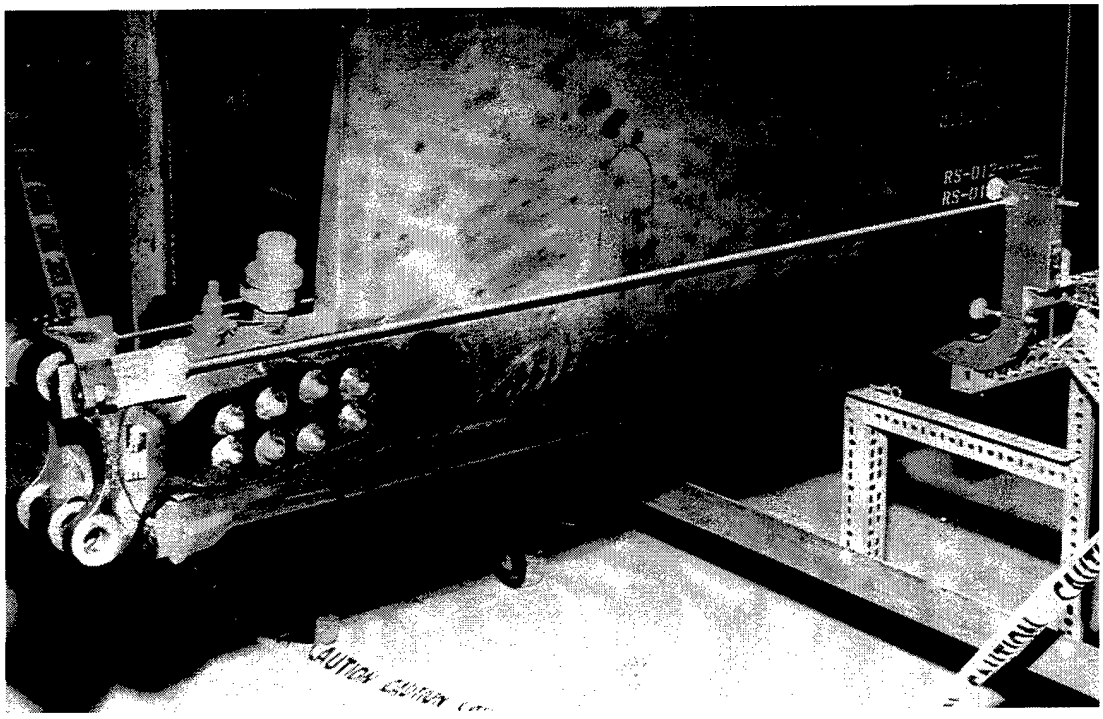

Figure 12. View of blade root positioning fixtures devised for Black Hawk blades

EXPERIMENTAL TEST PROGRAM

3.1 General Test Procedures

In all cases the tests consisted of three principal procedural tasks:

1) **Initiating the data acquisition program, TAKDATA2.** This program was written to enable the user to make data acquisition runs by responding to input prompts from the computer. Generally, the data input prompts were all in the form of commands to input various engineering quantities, and relate either to identifiers of output data files, to selection of input sensor (analog channel), or to operation of the A/D converter (number of points in stream of data, number of data streams, resolution bits, corner frequency of the low-pass filter, etc.). When data input was completed the operation of the data acquisition was automatic.

2) **Measuring the tare loads on the support cables.** This step was taken with the cradle empty for purposes of providing tare values to establish the characteristics of the test article by itself. The data acquisition unit provided for selective sampling of each of the five load cells, (4) static load cells, one on each of the support cable attachments, and the (1) dynamic load cell in series with one of the lateral springs. These tare loads were thus taken in the same way as the dynamic load cells.

3) **Measuring the weight and static properties of the cradle and test article.** For this step the test article (metric inertia bar or rotor blade) was installed in the cradle. The cradle was secured with the retention bolts screwed in, in order to load the cradle

4) **Manually establishing a suitable lateral oscillatory motion of the test article in the support cradle.** This motion must be large enough to ensure a long ring-down period and a maximum resolution signal from the load cell, and yet small enough to not hit on one of the amplitude limiting ends of the restraining bolts. The optimum motion to be achieved was to establish a quadrature phasing of the lateral translational motion with the rotational motion while minimizing all longitudinal motion. Once the proper motion was established, all contact with the oscillating body was avoided and the digitization was started, either using the manual trigger switch or by hitting of any key on the computer keyboard. Figure 13 shows this procedure in operation; note the testor's use of the hand-held digitization switch.

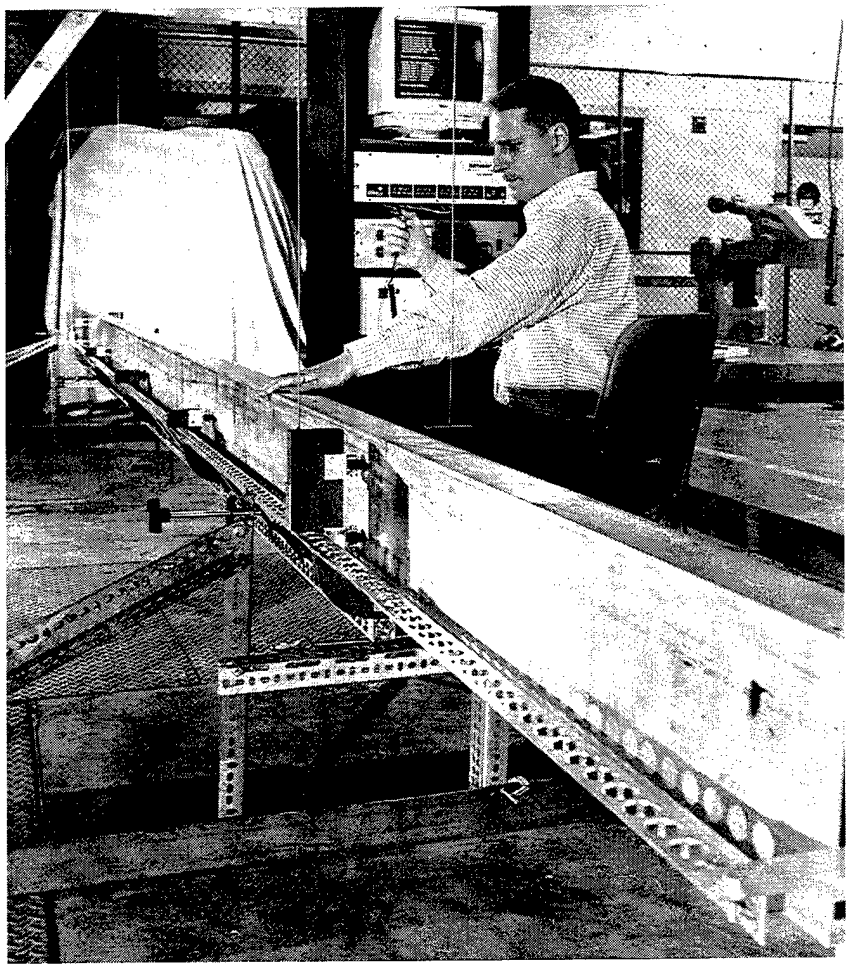

Figure 13. Illustration of procedure for manually establishing oscillatory motion and use of manual digitization switch

3.2 Tests with only the Support Cradle Assembly

Initial tests with the facility in the RPI test site were made with the support cradle assembly empty, for purposes of establishing an inertia "tare" that could be subtracted from the total results, so that the inertia properties of the test article by itself could be obtained. These tests were complicated by the fact that the cradle assembly is relatively light and the resulting rigid-body mode frequencies were high enough to couple with the "vibrating string" modes of the support cables. Subsequent substitution of softer lateral springs reduced the vibrating string mode coupling, but also reduced the oscillatory spring loads with commensurate reductions in load cell output level. This reduction in output level effectively reduced the resolution of the A/D converted signals so that the full potential for accuracy of the A/D converter could not be used.

3.3 Tests with the Metric Inertia Bar

All tests with the metric inertia bar were conducted in the same manner as described above. Since the weight of the inertia bar was significantly greater than that of the support cradle alone, (a) the tension in the support cables was greater, resulting in higher frequency vibrating string modes, and (b) the rigid-body rotational mode frequency was lower due to the increased inertia. Generally, the tests with the metric inertia involved attempting to select an optimum spring rate for the lateral springs. The softer springs produced relatively long time histories with less attenuation and little coupling with the support cable vibrating string modes, but they produced lower spring forces resulting in loss of signal resolution. The converse of these trade-offs exists with the use of the stiffer springs. One positive aspect of using the stiffer springs, however, is that less time then needs to be spent in acquiring the time-history transient responses, thereby leading to increased productivity which would reduce cost if the system were used in an actual manufacturing environment.

The objective of the present study was to establish practicality of the system, but not the optimize its implementation. Consequently, the eventual optimal implementation of the system would require an investigation into the interacting roles of: (a) the frequencies of response of the cradle and blade system, (b) the sampling frequency of the A/D converter, and (c) the resolution of the converter. As with the A/D converter used in the present study, it is to be expected that the sampling frequency would not be independent of the resolution of conversion. Also, the particular elements of any particular installation and the characteristics of the blades would be expected to play a role.

3.4 Ground-based Tests with the Black Hawk Rotor Blades

3.4.1 Objectives - The motivation for the testing of the Black Hawk blades was the supposition that variation in the moments of inertia among the blades in a set will result in blade track anomalies and consequently, one per rev vibration. The ground-based tests with the rig installed in the Sikorsky experimental high bay area had three objectives:

(1) Obtain weight, static moment and second moment values for a population of UH-60A/L blades that reasonably matched expected values.

(2) Show that the results are repeatable.

(3) Show that the correct results are obtained when a small known weight is added to the blade.

As is described in subsequent sections, all of the above objectives were met.

3.4.2 Scope of Test Program - Two initial tests were performed with the modified test rig to measure the first and second moments of the pin/positioning rod assembly. The blades were tested with the positioning hardware installed. These tests were conducted to determine mass properties of the assembly alone, which could then be subtracted from the test results to obtain the properties of the blade alone. After the inertia test facility was checked out, tests were conducted on a population of Black Hawk blades as described below:

Four flight test blades (s/n 1038 is an instrumented blade). These blades were built between 1981 and 1986.

One production blade (s/n 3764, built in 1985) that was never delivered. This blade was rewhirled at least three times after aircraft removals for one per rev problems.

Twenty-four production blades built in 1994 and 1995.

One blade tested with an additional weight on the blade (1.94 lb at 195.5 in from the reference point). This test was designed to test the ability of the rig to accurately detect a known, small inertia change.

3.4.3 Test Procedures - Details of the test setup and procedure used in the Sikorsky site tests generally followed the same basic test procedure outlined previously in Section 3.1. The following points summarize the process, as applied to tests with the rotor blades:

1) Take static data for the empty cradle.

2) Load the blade into the cradle. A set of fittings and rods were used along with a blade retention pin to position the blade correctly in a standardized longitudinal location.

3) Take static data for the cradle and blade.

4) Take ten streams of dynamic transient time history data.

5) Analyze the data. The static measurements were used to calculate the static or first moment. The dynamic data were used to calculate the second moment. The roots for each data stream were examined for consistency with the roots for other data streams; typically most were very close in frequency. The few that significantly mismatched the average were rejected from the inertia calculations.

3.5 Flight Tests with the Black Hawk Rotor Blades

For the blades tested on the ground with the pendular test facility, test flights were made with the blades installed on a Black Hawk helicopter in hover and at 145 knots. Vibration and out-of-track data were taken for the first flight (before one per rev adjustments were made), and then for a second flight after all one per rev adjustments were made and the one per rev vibrations were deemed acceptable.

4.0 EXPERIMENTAL RESULTS

4.1 Results Obtained in the RPI Test Site

4.1.1 Tests with the Support Cradle Alone - The basic test procedures described in Section 3.1 were used to measure the inertia characteristics of the support cradle alone. In this case the static load cell measurements used for the tare values were those obtained with the cables unattached to the support cradle. Initial tests were made with variations in A/D converter resolution, number of samples in the time streams, low-pass filter corner frequency, and spring configurations (using the "A" springs). These initial tests were unusable because the light-weight construction of the cradle together with the "A" springs produced natural frequencies high enough to couple with the "vibrating string" modes of the support cables. Consequently, a set of significantly softer springs (the "E" springs) was obtained and used to obtain successful results.

Although the design and fabrication of the support cradle employed generally regular geometric components, a separate analytic calculation of the inertia characteristics of the cradle was not made. Reasons for this omission were that: (1) the time and effort to validate the program written to make the calculations, make the appropriate measurements of the components, create and check the data file, etc., were beyond the time resources of the program, and (2) the inertia characteristics of the cradle were small fractions of those of the total test mass (cradle and test article) and could thus be assumed to play a small role in the accuracy of measurements of the test articles. This is especially true for the population of rotor blades tested at the Sikorsky site where tests were made more for consistency between blades and not for absolute inertia values, per se. Thus, the results presented in the following table are those measured and used as tare values with subsequent test of the actual test articles.

Table 3. Measured properties of the support cradle assembly

Property	Value	Units
weight	31.52	lb
S_{x_1}	3,283.2	lb-in
$x_{c.g.}$	104.16	in
I_{zz_1}	517,707.	lb-in^2
$k^2_{zz_1}$	16,426.29	in^2
$k^2_{zz_0}$	5,578.1	in^2
k_{zz_1}	128.17	in
k_{zz_0}	74.687	in
$(k_{zz_0} / L)^2$	0.1513	ND

4.1.2 Tests with the Metric Inertia Bar - Three sets of tests were made with the metric inertia bar, corresponding to the use of three sets of lateral attachment springs (with increasing stiffness): the "E", "A", and "B" springs. In each of the tests the first order of business was establishing the values of the two natural frequencies. This procedure was typically accomplished in a trial and error basis, varying the filter corner frequency and the degree of resolution until repeatable frequencies were detected. Once these frequencies were known, the corner frequency was set at a range near to and ranging about the lowest of the two natural frequencies. Generally, (10) streams of data were taken for each data point, and the eigenvalues used in the regression analysis were the average of those whose frequencies were deemed to be consistent and thereby includable in the average.

Figure 14 presents the first of the results achieved for the softest set of springs ("E" springs), showing the effects of variation in the low-pass filter corner frequency about the clustered values of the two natural frequencies. Also plotted on this figure and all of the figures discussed in this section is the analytically calculated value for the square of the nondimensionalized radius of gyration as given previously in Section 2.3, for

comparison. Note that in all the results relating to variation of low-pass corner frequency, this parameter was variable only in 0.1 HZ increments. Thus, limited variationaly results were achievable at the low frequencies characteristic of this test rig.

Figure 14 confirms the trend found in Reference 1, namely that the accuracy of the algorithm tends to fall off for filter corner frequencies significantly below and above the clustered range of the natural frequencies. Also, the figure presents generally excellent correlation with the analytical value. This evaluation must be qualified, however, by virtue of the fact that the analytical value is an approximation.

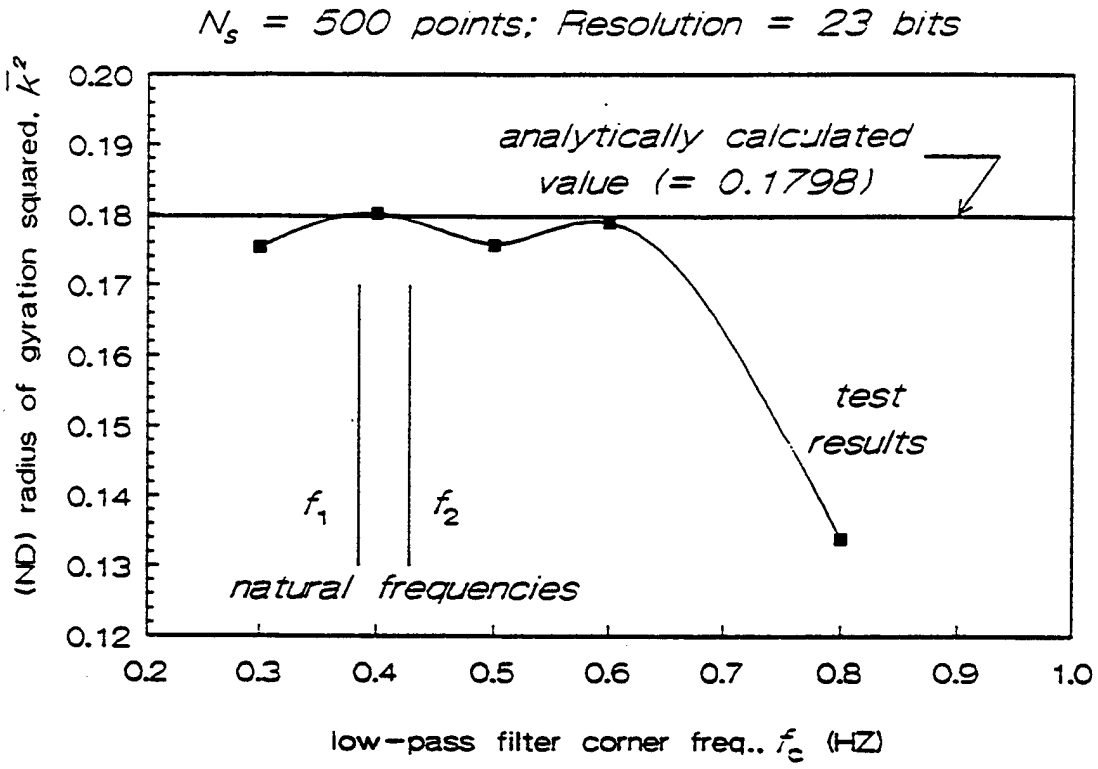

Figure 14. Effect of low-pass filter corner frequency on radius of gyration squared characteristics for metric inertia bar, "E" springs: $gK_1 = gK_2 = 207\ lb_f/s^2$

The A/D board used did not have much variation available in the number of bits of resolution at the high end. Figure 15 presents the results for essentially the only two valid data points achieved with a variation on this parameter. Note that the 22 bit result in the

figure is nonnumerical, indicating only that the algorithm implementing Prony's method broke down for that case. For the A/D board, resolution bit values of 22, 23, and 24 correspond, respectively, to sampling rates of 7.5, 3.75, and 2 samples/sec. Thus, there appears to be a "tuning" process at work for the need for a high enough sampling rate and at the same time a high enough degree of resolution for the algorithm to work.

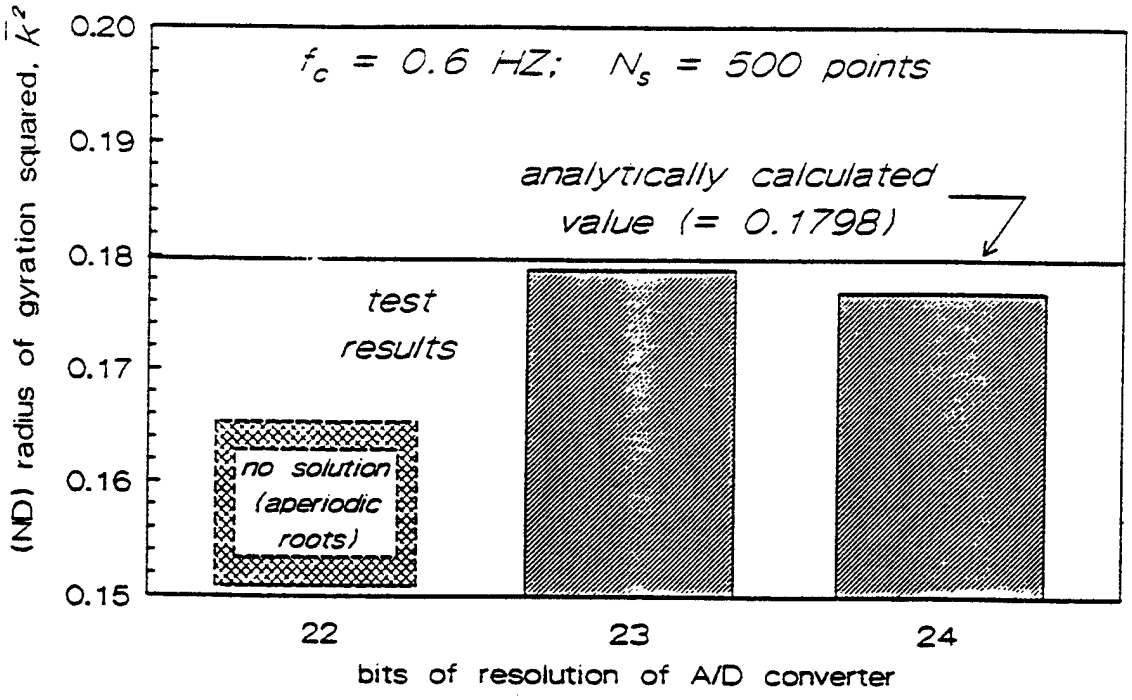

Figure 15. Effect of A/D resolution on radius of gyration squared characteristics for metric inertia bar, "E" springs: $gK_1 = gK_2 = 207\ lb_f/s^2$

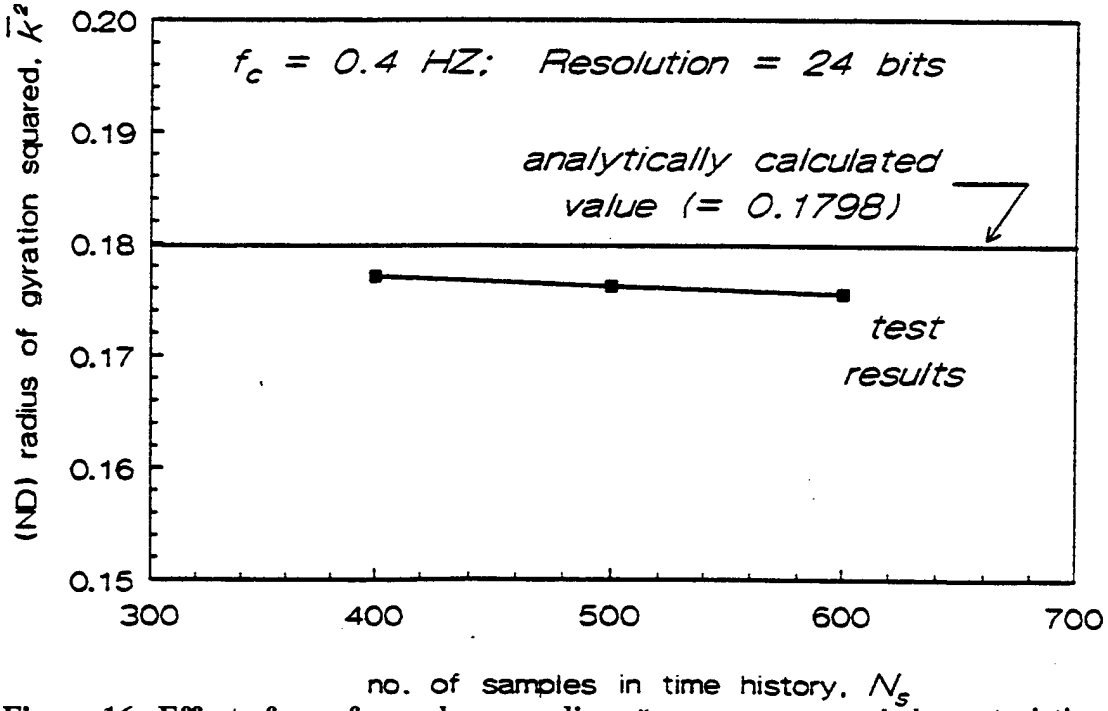

Figure 16. Effect of no. of samples on radius of gyration squared characteristics for metric inertia bar, "E" springs: $gK_1 = gK_2 = 207\ lb_f/s^2$

Figure 16 presents the results achieved with a variation on the number of samples taken in each of the data streams taken. The figure shows that, for this range of numbers of samples, the results are reasonably accurate, yet insensitive to this variable.

Figures 17 and 18 present the results achieved with the "A" springs with regard to variations in filter corner frequency and numbers of samples in the time history. Generally, for this stiffer spring configuration, little variation is seen in the results for these parameter variations. Note that for this configuration the higher sampling frequency mode (22 bit resolution) now gives a realistic prediction, but the accuracy is not as good as that for the 23 bit resolution case.

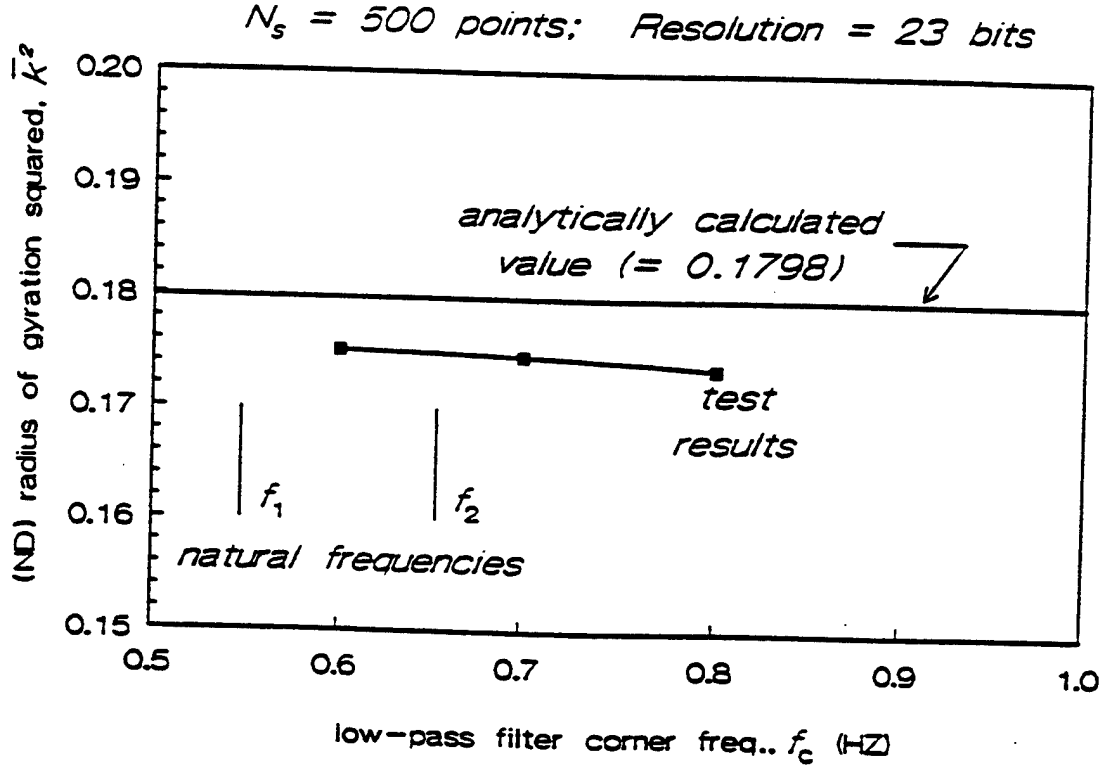

Figure 17. Effect of low-pass filter corner frequency on radius of gyration squared characteristics for metric inertia bar, "A" springs: $gK_1 = gK_2 = 575$ lb_f/s^2

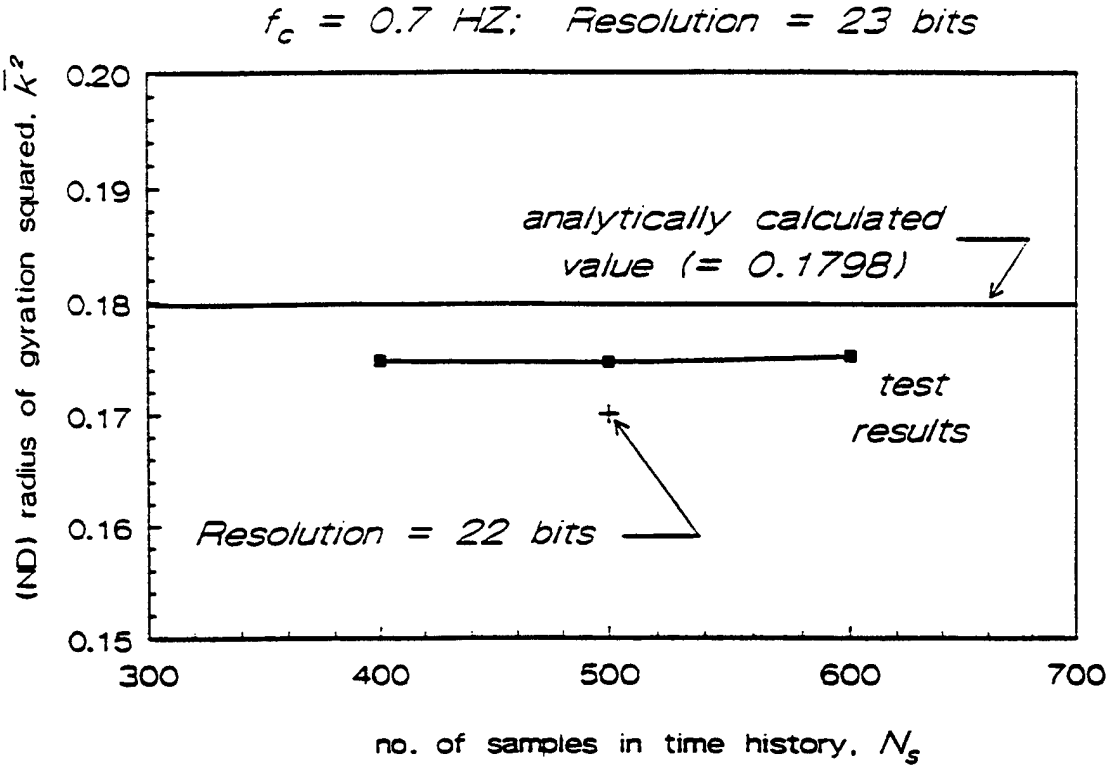

Figure 18. Effect of number of samples on radius of gyration squared characteristics for metric inertia bar, "A" springs: $gK_1 = gK_2 = 575$ lb$_f$/s^2

Figures 19 and 20 present the results for the highest of the spring rate cases investigated. For this inherently higher frequency configuration, it appears that the accuracy is relatively insensitive to the use of 22 or 23 bit resolution and indeed, because of this insensitivity, the 22 bit mode of operation was used for most of the cases since they took less time to acquire the data. Again, the results of varying the number of samples in the time history show little sensitivity to this parameter.

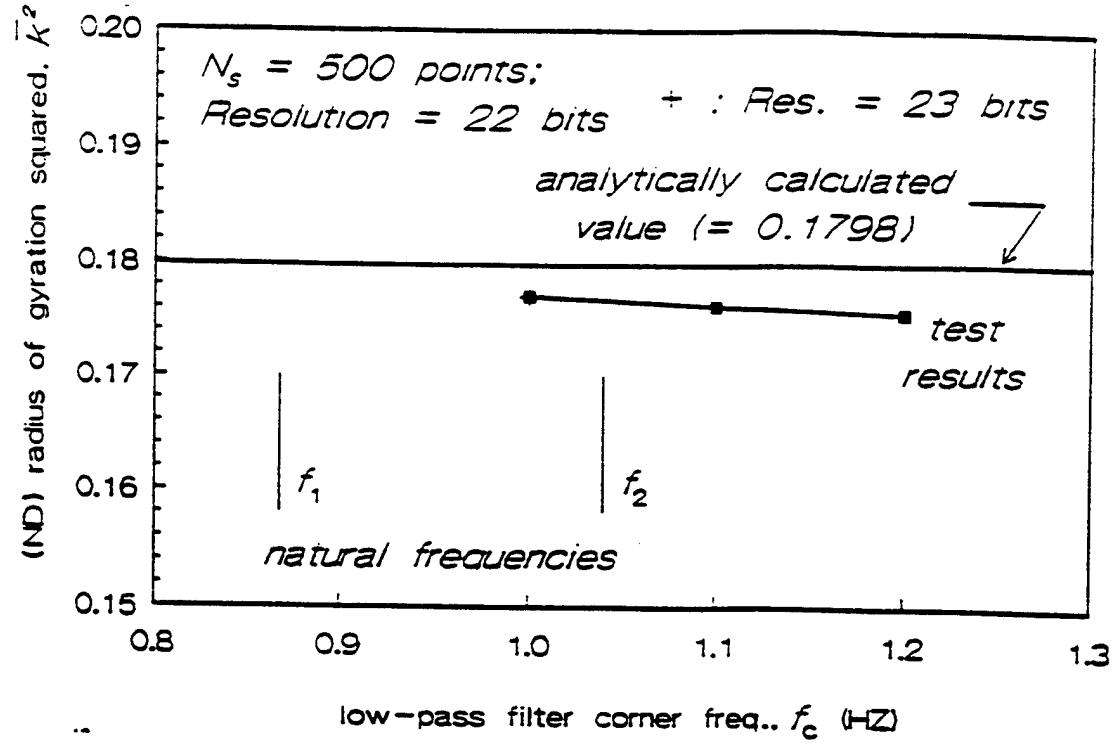

Figure 19. Effect of low-pass filter corner frequency on radius of gyration squared characteristics for metric inertia bar, "B" springs: $gK_1 = gK_2 = 1585$ lb$_f$/s^2

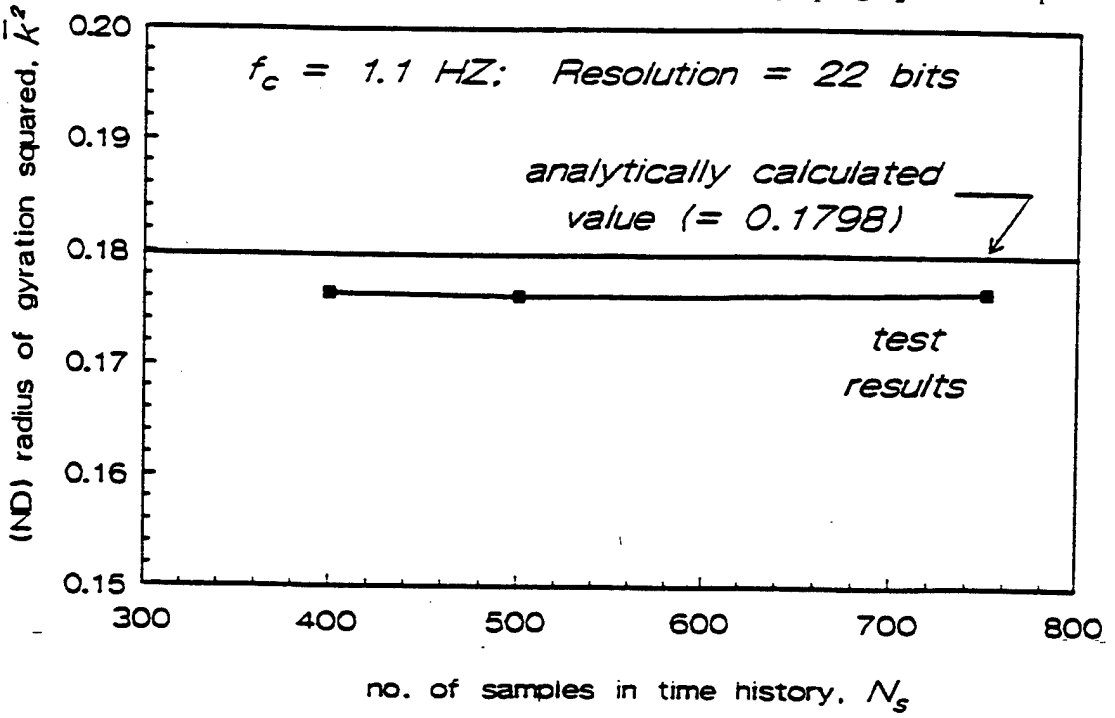

Figure 20. Effect of number of samples on radius of gyration squared characteristics for metric inertia bar, "B" springs: $gK_1 = gK_2 = 1585$ lb$_f$/s^2

4.2 Results Obtained in the Sikorsky Test Site

Once the rig had been relocated, set up in the experimental bay area and confidence in the test facility was achieved, testing of the Black Hawk blades was initiated. These tests were conducted principally to investigate the variation in moment of inertia of a population of blades. A total of twenty-four production blades were tested. In all of the tests at the Sikorsky test site the static (support cable) load cell data was acquired using 100 samples in the time stream, with the A/D converter configured with the full 24 bit resolution. For all the dynamic time stream data, the data streams were 500 samples long, the A/D converter was configured with 23 bits of resolution, and the low-pass filter configured with a corner frequency of 1.0 HZ.

4.2.1 Measurement of Blade Positioning Assembly Inertia - The blade inertia tests were done with the positioning hardware in place. The analysis procedure subtracts the tare values for the cradle but these tares do not include the positioning hardware. As a result, the weight and inertia values in the attached tables and figures include both the blade and the positioning hardware. In an attempt to obtain values for the incremental inertias of these extraneous parts, two blades were tested with and without the pin/positioning rod assembly. Since a great deal of the weight of this assembly is due to the pin (2.16 lb), which is at the reference point, the inertia effects are quite small compared to the values for the entire blade. For the two tests of the pin assembly inertia, the inertias without the pin were subtracted from those with the pin. The resulting inertia values for the pin assembly shown below, were not very consistent. If more testing is done in the future, this test of the positioner effect can be repeated to get better values or (preferably) the rod assembly could be used to position the blade and then be removed when the blade tests are conducted. The results of these experiments are shown below. The values listed are the differences between the values measured with the blade and pin assembly and those measured with the blade only (units are appropriate combinations of lb and ft):

Δ(quantity)	Blade 9525	Blade 3764	Direct weighing
Weight	3.87	3.91	3.78
First moment	55.67	70.75	
Second moment	19,687.5	9592.5	

4.2.2 Correlation of First Moment Measurements with Known Value - The first moment of the master blade is 35,418 in-lb about the center of rotation (CR) (this is a measured value from the blade static balance scale). The center of the blade retention pin is the reference axis for the blade inertia test data. This pin is 30 inches from the CR. If the mean measured static moment is transformed to the CR, the moment is 35,554 in-lb. Subtracting the average value of the measured pin assembly static moment (about the CR) results in a static moment value of 35,377 in-lb which is within 41 in-lb or 0.11% of the accepted value for the master blade.

4.2.3 Correlation of Second Moment Measurements with Predicted Values - The KTRAN UH-60 rotor deck was modified to remove all mass inboard of 30 inches, leaving only the mass of the blade as tested in the inertia rig. The sum of the weight values for this case is 210.07 lb which matches very well the test weight (minus the positioning rod assembly) value of 210.02 lb. The calculated static moment about the inertia test reference axis is 29,499.5 in-lb. The mean test value, minus the average of the measured static moment of the pin assembly, is 29,066.8 in-lb which is 1.47% lower than that given by the analytical model. The calculated mass moment of inertia about the inertia test reference axis is 5,602,000 lb-in^2. The mean test value, minus the average of the measured inertias of the pin assembly, is 5,912,063 lb-in^2 which is 5.5% higher than that given by the analytical model. This discrepancy may result from a systematic error in the test rig, or from inaccuracy in the analytical model of the weight distribution.

4.2.4 Measurement of a Small Change in Inertia - Blade 4392 was retested with an added 1.94 lb weight attached to the cradle at a spanwise location 195.5 inches from the pin. The calculated and measured changes in mass properties are shown below:

Δ(quantity)	Analytical	Measured
Weight	1.94	1.94
First moment	379.27	362.4
Second moment	74,147	89,044

The measured values are reasonably close to the expected values but based on the results of the repeatability tests and the correlation of the blade weight and inertias with expected values, the errors in this experiment are higher than expected.

4.2.5 Repeatability Tests - Two blades were tested twice to evaluate the repeatability of the measurements. In each case, the blade was removed from the test rig between measurements and, for blade 902, the tests were done on different days. For blade 3772 the difference between the first and second tests were 0.013% and 0.064% for first and second moment, respectively. For blade 902 the differences were 0.009% and 0.066%. For this limited sample, the results show excellent repeatability and provide confidence that the small differences seen among the production blade results represent physical differences in the blades rather than measurement scatter.

4.2.6 Summary of Blade Population Characteristics - Figures 21 through 23 present a summary of the measured weight and inertia characteristics for the 24 blades tested.

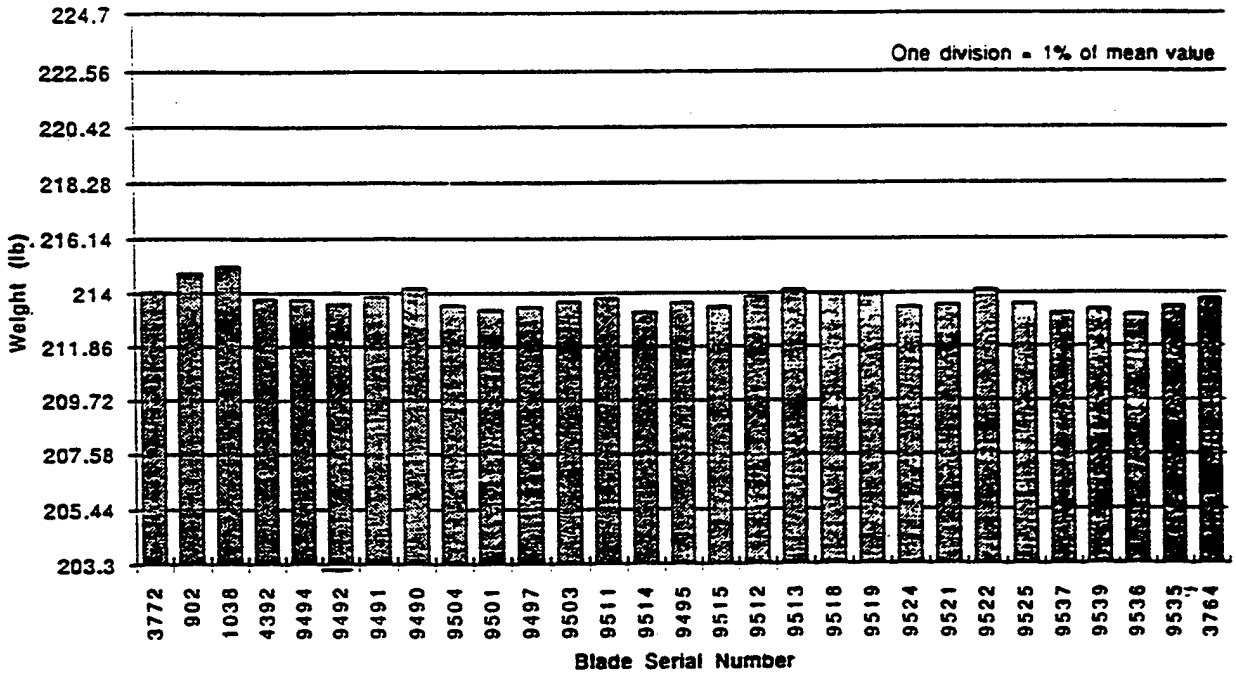

Figure 21. Weights of population of UH-60 main rotor blades

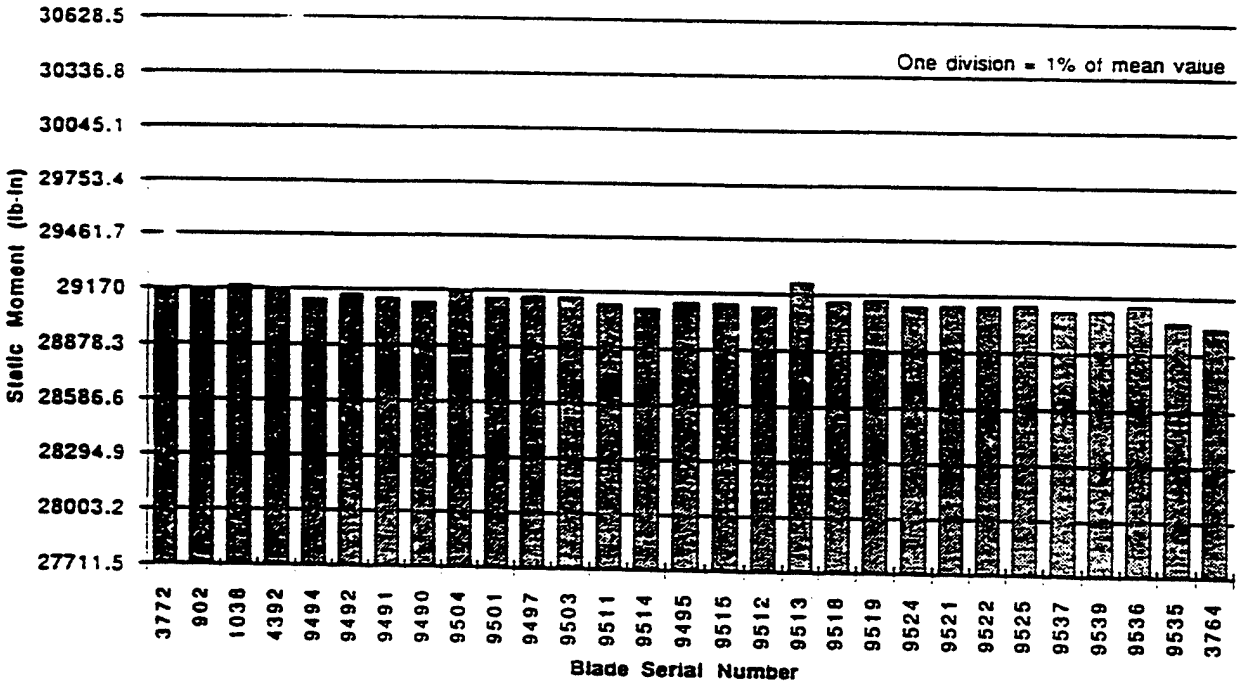

Figure 22. Static moments of population of UH-60 main rotor blades

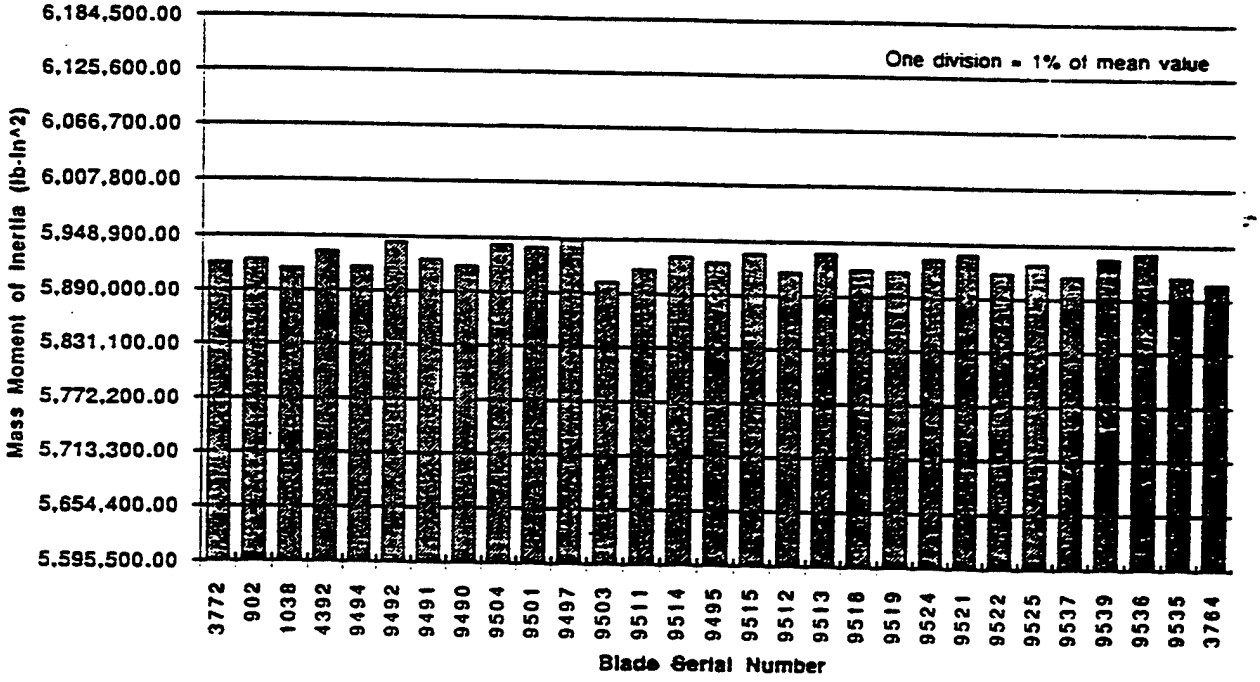

Figure 23. Mass moments of inertia of population of UH-60 main rotor blades

Generally, the preceding figures show that:

1) Although there is some minor variation in the weights of the blades, the blades have quite uniform first mass moments (as should be the case after the blades have been balanced).

2) There is little variation in the second mass moments. The mass moments of inertia for these blades were all found to be within $\pm$ 0.5% of the mean.

4.2.7 Flight Test Results - Acceptance test track and vibration data were obtained for six aircraft that each flew with one of a set of four of the blades that were tested with the rig (and identified in Figures 21 through 23). Sets of scatter plots of these data are presented in Figures 24 through 27. Each of these figures shows the measured blade track results versus measured mass moment of inertia for the blade. It should b noted that these measured track results are obtained at only one rotor azimuth and, except for hover (mainly, but not entirely), are not true measurements of the steady out-of-track condition that moment of inertia dissimilarity effects will produce.

Figures 24 and 25 present the measured blade track characteristics, respectively, in hover and at 145 knots flight in the first flight before any 1/rev reduction adjustments have been made. Figures 26 and 27 present the same type of measured blade track characteristics for the same blades, again respectively, in hover and at 145 knots flight, but after the 1P adjustments have been made and the 1P vibrations were deemed acceptable. In the process of making routine hub weight, pitch change rod and trim tab corrections on these aircraft, no anomalies were noted in the response to adjustments.

Included in these figures is the slope of steady track change per moment of inertia change, based on results of Reference 1. Specifically, all other things kept constant, the change in coning is related to the change in moment of inertia by the relationship:

$$\Delta\beta_0 = = \Delta z_{tip} / R = -\frac{\Delta I_b}{I_b + eS_b}\beta_0 \qquad (11)$$

For a typical coning angle of 3.5 deg. resulting slope, $\Delta z_{tip} / \Delta I_b$, is -7.85 x 10^{-5} mm/lb-in^2.

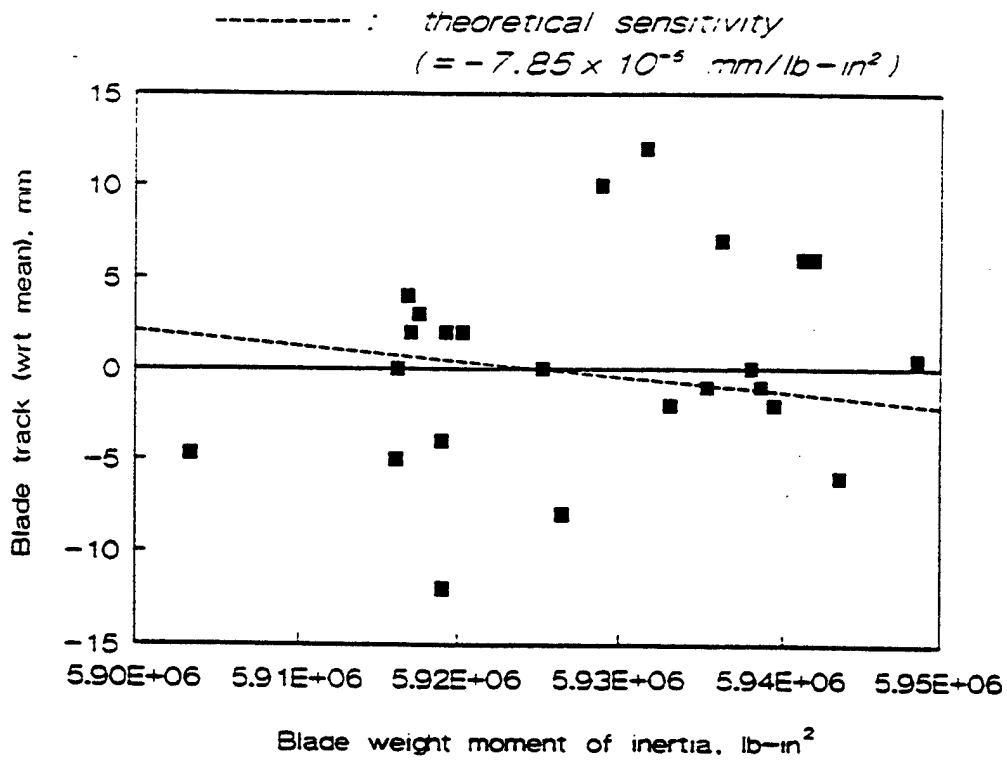

Figure 24. Hover track characteristics vs. flapping moment of inertia, first flight tests.

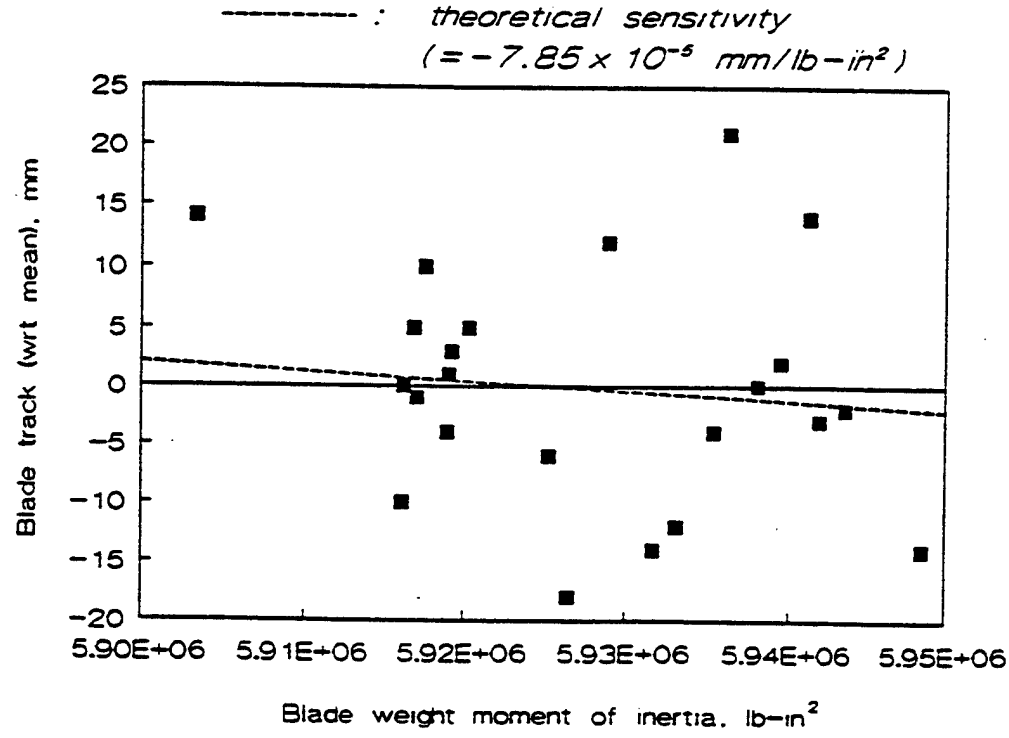

Figure 25. 145 knot track characteristics vs. flapping moment of inertia, first flight tests.

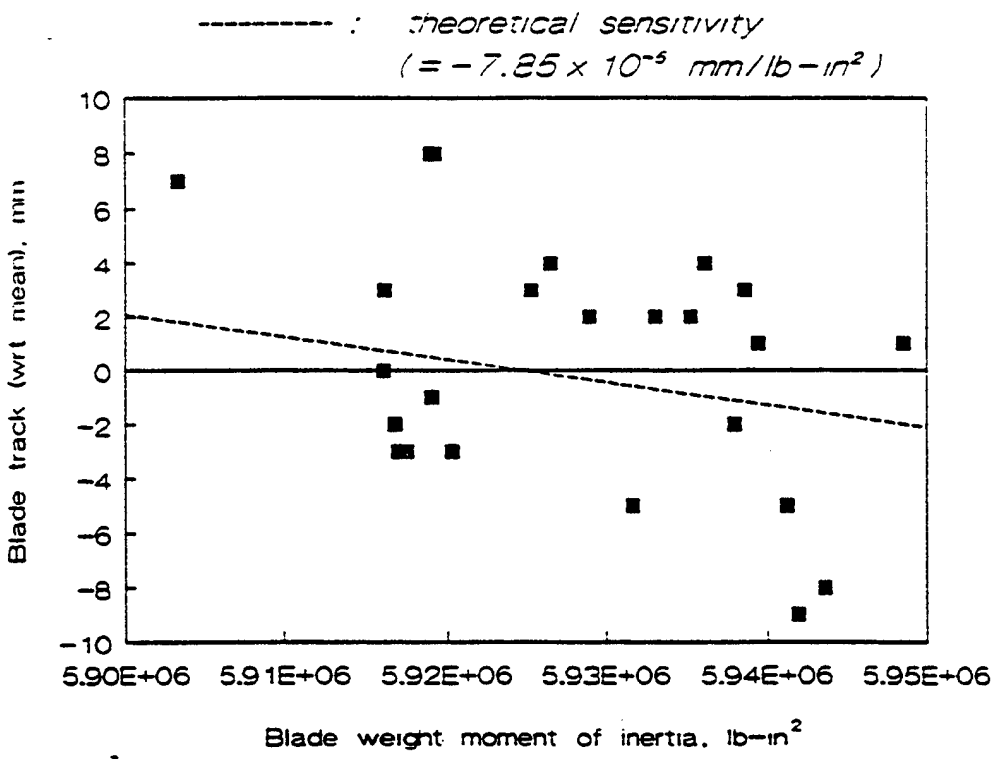

Figure 26. Hover track characteristics vs. flapping moment of inertia, after 1P acceptance flight tests.

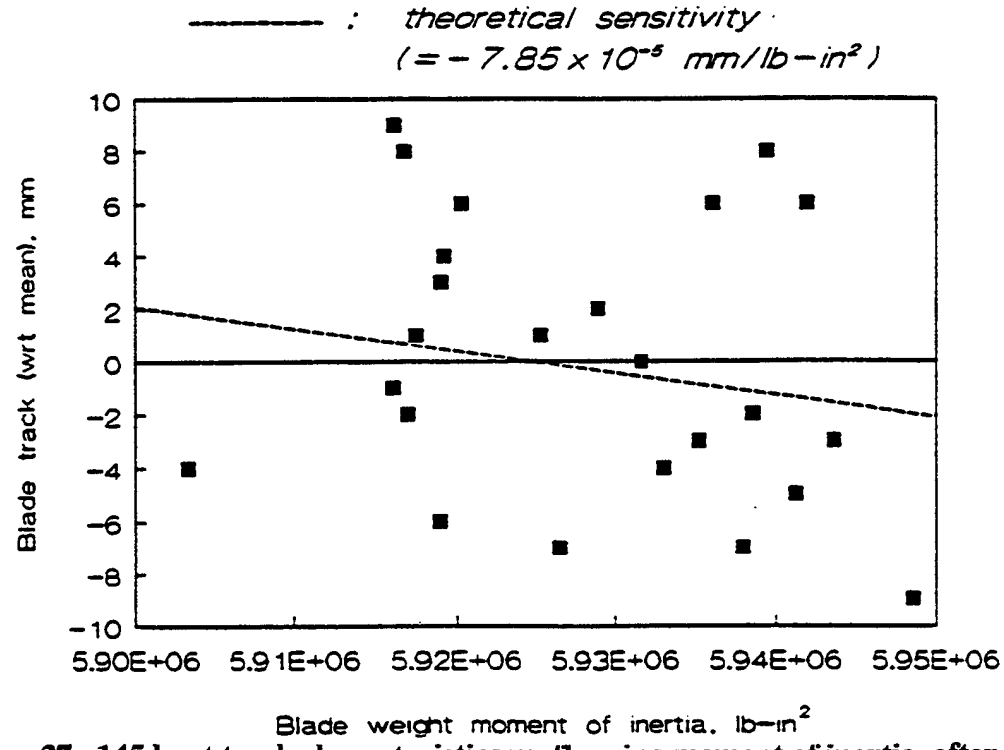

Figure 27. 145 knot track characteristics vs. flapping moment of inertia, after 1P acceptance flight tests.

Observations of the results presented in these figures are:

1) There is no obvious correlation between the inertia and the blade track and vibration.

2) There is no obvious correlation between the track characteristics in hover and at 145 knots.

3) For the blades tested, the out-of-track characteristics due to inertia dissimilarities are much smaller than those due to other sources. As the results of using Equation 11 indicate, this may be due to the variation in inertia being relatively small for this population of blades.

It is suspected that older blades can have more mass variation because of repairs, paint erosion, repainting, water absorption or other factors. These effects were partially investigated by testing five older blades one of which had been rejected repeatedly from production aircraft because of vibration problems. The mass moments of inertia of these blades were within the range of values measured on the new blades.

4) The ability to fine tune the blades to arbitrarily small amounts of out-of-track even in hover is quite limited. Thus, non-inertia-related sources of out-of-track that are relatively large compared to the inertia-related sources would remain large.

5.0 CONCLUSIONS

5.1 General Conclusions

The following general conclusions are drawn from the experimental results:

(1) The flapping inertia characteristics of helicopter rotor blades can be accurately measured with the pendular system.

(2) The results are repeatable.

(3) The newly configured extraction algorithm is an improvement over that presented in Reference 1 in that it allows for the use of a separately acquired static moment measurement, minimizes the sensitivity of the gravitational acceleration, and generally appears to be more robust.

(4) The instrumentation required to obtain the inertia measurements is well within the available state-of-the-art. Furthermore, the system lends itself well to exploiting this state-of-the-art.

(5) The physics governing the role of the key data acquisition parameters is not well understood and the identification of the conditions for an optimized system still need to be addressed. For example, the lower limit of samples per time stream for accuracy was not addressed.

(6) Although the pendular system provides the ability for improved quality control based on blade moment of inertia, in addition to the usual blade static moment, it is still not enough to assure arbitrary reductions in out-of-track induced 1P vibrations.

(7) The system is presently only a laboratory facility, and is not yet design-optimized for practical cost-effective use in a manufacturing environment. Much needs to be accomplished to bring it to this state before an objective evaluation of its merit in a production facility can be assessed.

5.2 Specific Conclusions

5.2.1 As Relate to the Practicality of the Inertia Measurement System - The following issues are identified as a result of the tests performed:

(1) A more accurate weighing system should be devised for load cells at the tops of the support cables whereby the amplifier and load cell offset and gain drifts are strictly minimized along the lines of modern load cell based laboratory weight scales.

(2) The instrumentation used for measuring the support cradle assembly alone characteristics should have the capability for increasing the gain of the load cell output to the A/D converter, in order to use the resolution characteristics of the A/D converter more fully.

(3) Support cables should be free of kinks and/or bends.

(4) Ways should be devised to measure the cradle-alone characteristics without exciting the "vibrating string" modes of the support cables. One method might be to constrain the pairs of end cables together with a light-weight spacer transverse to the cables.

(5) Future (more operational) test facilities need to have the top support carefully plumbed to ensure that a level cradle assembly is consistent with equal cable lengths.

(6) Although not extensively used in this study, the use of ultra-accurate, laser-based measurements of critical lengths needs to be thoroughly addressed.

5.2.2 As Relate to the Applicability to Actual Helicopter Rotor Blades - The following observations have been made based on the results with the sampling of relatively new rotor blades:

(1) The variation in mass moment of inertia on new UH-60 Black Hawk blades is fairly small. Stated differently, the out-of-track characteristics due to dissimilarities in blade mass moment are small compared to the characteristics due to non-mass moment of inertia effects, e.g., aerodynamic dissimilarities, dissimilar torsional stiffness and/or torsion-axial extension elastic coupling effects. Note that the inertia of a known one/rev problem blade was found to be within the range observed for new blades that behaved well.

(2) For the Black Hawk rotor blades quality control appears to have been consistently maintained in that the mass properties of five older blades are within the same range as the new blades.

(3) The root of the blade (and not the blade tip) should be used for accurate longitudinal positioning of the blades in the support cradle.

(4) Ways to make the system more "user-friendly" should be explored. The use of rollers to expedite the entry of rotor blades into the cradle assembly should be included.

(5) It is still not known whether blades may exist with larger second mass moment variation and whether such variation would cause uncorrectable blade track or vibration problems.

(6) The opportunity to make a scientifically sound assessment of the role of mass moment of inertia control as a means for 1P vibration control was missed. The originally defined test plan was to fly one set of blades with a close match on both mass moment of inertia and static moment and record the helicopter's vibration characteristics. Then one blade with significant dissimilarity in only the second mass moment was to be substituted for one of the original well-tuned set and the helicopter again flown and tested for 1P vibration. It is understood that such an approach would be more expensive than what was actually done, but the value of the flight tests performed is significantly less than it could have been.

6.0 RECOMMENDATIONS FOR FUTURE WORK

1) Conditions for an optimized system should be studied. One element of an optimal system is that of cost-effectiveness, and an important element of cost-effectiveness is the minimization of the amount of time required to make the measurements. The amount of time needed to make sufficiently accurate measurements is dependent on the frequency of motion and the sampling time/digitalization resolution characteristics of the A/D converter used. Another element of the cost-effectiveness of the system relates to the availability of an area for blade quality testing with a sufficiently high ceiling to suspend the system and retain linearity in the system response.

2) In further tests with the present rig, tests for repeatability and comparison to known or independently verifiable values should be continued. The use of enhanced capability, high resolution, yet higher speed A/D converters to enable greater independent variability in resolution and sampling rate should be explored. Attempts should be made to understand the sources of errors and/or variability.

3) Also with regard to further tests with the present rig, the cradle should be modified to include a set of rollers and an improved positioning guide design to facilitate blade entry to and egress from the cradle so that practical and convenient usage can be made of the rig.

4) Mass moments of inertia of some blades from the field that have been repaired, repainted or have caused vibration problems should be tested, in as much as such blades would be expected to manifest more significant variations in mass moment characteristics.

5) A blade with a known, fairly large perturbation to its mass moment of inertia and with a static moment at its nominal value should be flight tested to determine empirically the effects on track and vibration and the degree to which we can correct for such an anomaly with hub weight, pitch change rod and tab adjustments.

7.0 REFERENCES

1. Bielawa, R.L., Development of a System for Improved Helicopter Blade Tracking, Phase I, Final Report, RTC Report D-93-1, Rensselaer Polytechnic Institute, June, 1993.
2. Margenau, H., Watson, W.W., and Montgomery, C.G., *Physics, Principles and Applications*, McGraw-Hill Book Company, New York 1953.
3. Hildebrand, F.B., *Introduction to Numerical Analysis*, McGraw-Hill, New York, 1956.
4. Baumeister, T. and Marks, L.S., (editors), *Standard Handbook for Mechanical Engineers*, Seventh Edition, McGraw-Hill Book Company, New York 1967.

APPENDIX A - Revised Equations of Motion

A.1 Formulation of Equations of Motion

The basic equations of motion for the two-degree-of-freedom system simulation of the inertia test rig were originally derived in the Phase I part of this developmental project and that derivation is presented in Reference 1. T=During the Phase II part of the project certain refinements and modifications to the use of the equations became necessary; this appendix presents a rederivation of the equations with these refinements and modifications included. The equations are still relatively straightforward but a Lagrangian approach was used instead. Figure A.1 shows the forces and moments acting on the cradle/test article assembly (as viewed from above) from which the equations of motion can be derived.

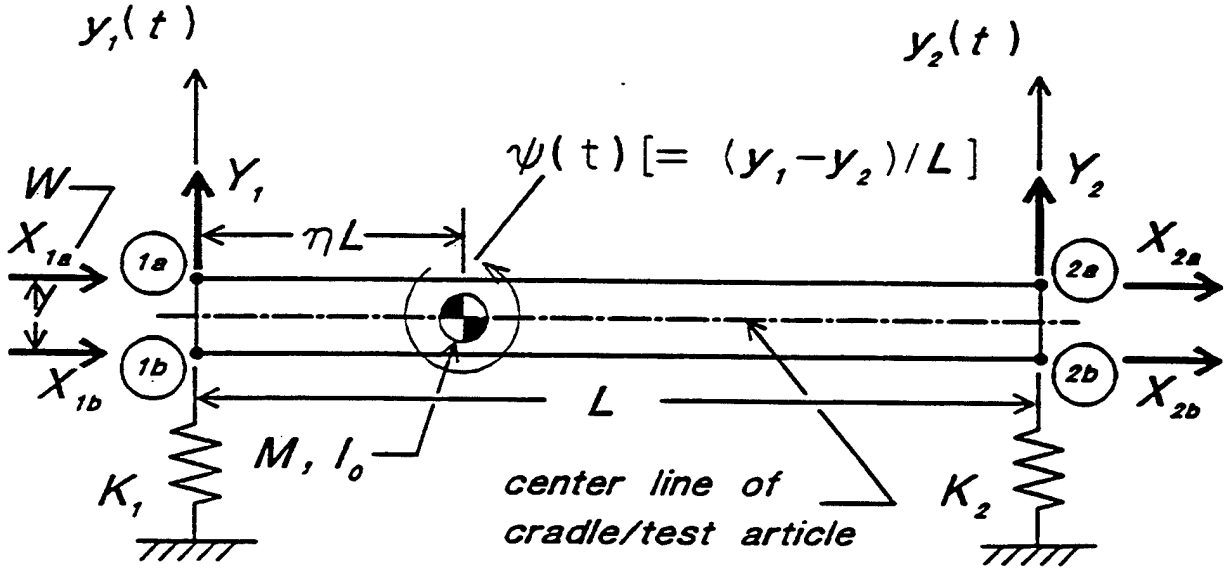

Figure A-1. Top view of force and moment schematic of cradle/test article assembly.

Differences in the development relative to that of Reference 1 are as follows:

1) The spring rates K_1 and K_2 are expressed as products with the gravitational acceleration g: (gK_1) and (gK_2). With this representation the normalized spring rates, $\bar{K}_1$ $(= K_1/M)$ and $\bar{K}_2 (= K_2/M)$ are now expressible in terms of the total metric weight, W_T:

$$\bar{K}_1 = K_1/M = (gK_1)/W_T \qquad \text{(A.1a)}$$

$$\bar{K}_2 = K_2/M = (gK_2)/W_T \qquad \text{(A.1b)}$$

The principle reason for this approach is that, for all the system components, it is generally easier to measure weight than mass. Consequently, the rederived equation set is less sensitive to the exact value of the gravitational constant, g. Also, the most accurate way of measuring *dynamic* spring rates of K_1 and K_2 is, for each spring under consideration, to measure the variations in natural frequency of the resulting spring–mass system, ω_S, with known incremental variations in added weight, δW ($= \delta g M$). Specifically, the resulting variation of $1/\omega_S^2$, with incremental added weight ideally produces a straight line whose slope is $(gK)^{-1}$.

2) The weight of the cables is explicitly considered, in as much as the motion of the cables is different from that of the combined cradle/test mass. The cable mass is assumed to be distributed equally between four identical wires (each a line mass with uniform mass distribution).

3) The springs also contribute mass, but this mass can be considered to be part of the combined cradle/test mass and thus, extractable from the final results, as is presented in Sect. A.4.

4) The effective translational damping is assumed to act at the *geometric center* of the cradle/test inertia rather than at the center of gravity

A straightforward application of Lagrange's equations requires the definition of the kinetic energy, the potential energy, the generalized forces and the dissipation function. Formulated expressions for these quantities are presented in the following equations:

Kinetic energy:

$$2T = I_0\left[\frac{\dot{y}_2 - \dot{y}_1}{L}\right]^2 + M\left[(1-\eta)\,\dot{y}_1 + \eta\,\dot{y}_2\right]^2 + \frac{1}{2}m_w\left[\left[\frac{\dot{y}_1}{2}\right]^2 + \left[\frac{\dot{y}_1}{2}\right]^2 + 2\left[\frac{W}{4}\dot{\psi}\right]^2\right] + m_w k_w^2\left[\left[\frac{\dot{y}_1}{H}\right]^2 + \left[\frac{\dot{y}_1}{H}\right]^2 + 2\left[\frac{w}{2H}\dot{\psi}\right]^2\right] \tag{A.2}$$

where m_w k_w are, respectively, the total mass of the support cables, and the radius of gyration of a cable about its midpoint (i.e., mass center).

Potential energy:

$$2U = K_1 y_1^2 + K_2 y_2^2 \tag{A.3}$$

Generalized forces:

$$\delta W = Y_1\,\delta y_1 + Y_2\,\delta y_2 + (X_{1_b} + X_{2_b} - X_{1_a} - X_{2_a})\frac{w}{2}\delta\psi - \frac{1}{2}m_w g\frac{H}{2}\left[\phi_1\,\delta\phi_1 + \phi_2\,\delta\phi_2\right] - m_w g\frac{H}{2}\phi_\psi\,\delta\phi_\psi \tag{A.4}$$

where the angular deflections of the cables are given by:

$$\phi_1 \equiv \frac{y_1}{H} \tag{A.5a}$$

$$\phi_2 \equiv \frac{y_2}{H} \tag{A.5b}$$

$$\phi_\psi \equiv \frac{W}{2H}\left[\frac{y_2 - y_1}{L}\right] \tag{A.5c}$$

and where the X and Y cable forces, as depicted in Figure A-1, are defined by the following expressions:

Forces in the x-direction at the "blade root" end:

$$X_{1_a} = \left[\frac{W}{4H}\right](1-\eta)\, gM\, \psi \tag{A.6}$$

$$X_{1_b} = -X_{1_a} \tag{A.7}$$

Forces in the x-direction at the "blade tip" end:

$$X_{2_a} = \left[\frac{W}{4H}\right]\eta\, gM\, \psi \tag{A.8}$$

$$X_{2_b} = -X_{2_a} \tag{A.9}$$

where the yaw angle of the assembly mass is given by:

$$\psi = (y_2 - y_1)/L \tag{A.10}$$

Forces in the y-direction at the "blade root" end:

$$Y_1 = -(1-\eta)\, gM \frac{y_1}{H} \tag{A.11}$$

$$Y_2 = -\eta\, gM \frac{y_2}{H} \tag{A.12}$$

Dissipation function:

$$2D = B_1\left[\frac{\dot{y}_2 + \dot{y}_1}{2}\right]^2 + B_2\left[\frac{\dot{y}_2 - \dot{y}_1}{L}\right]^2 \tag{A.13}$$

A.2 Eigenvalue Solution

From the above expressions the two differential equations of motion can be derived with a straightforward application of Lagrange's equations. Since the resulting equation set will be linear, for present purposes, the direct solution of these equations would be accomplished by finding the eigenvalues, λ ($= \sigma \pm i\omega$). A wide selection of powerful matrix eigenvalue solutions presently exists. However, since the dynamic system only includes two degrees of freedom, it is practical to work instead with the characteristic equation wherein the eigenvalues are analytically related to the system parameters. Therefore, since the characteristic equation is actually of primary importance, the explicit statement of the equations of motion are omitted herein and are left as an exercise for the discerning reader. The resulting characteristic equation is as follows:

$$A_4\lambda^4 + A_3\lambda^3 + A_2\lambda^2 + A_1\lambda + A_0 = 0 \tag{A.14}$$

where:

$$A_4 = \bar{k}^2 + \tfrac{1}{4}\left[\left[\frac{m_w}{M}\right]\left[\tfrac{1}{4} + \bar{k}_w^2\right]\right]^2 (1 + \bar{W}^2) + \left[\frac{m_w}{M}\right]\left[\tfrac{1}{4} + \bar{k}_w^2\right]\left[\tfrac{1}{2} - \eta\,(1-\eta) + \frac{\bar{W}^2}{4} + \bar{k}^2\right] \tag{A.15}$$

$$A_3 = 2\bar{B}_1\left[\bar{k}^2 + \left[\tfrac{1}{2} - \eta\right]^2\right] + \bar{B}_2 + \left[\frac{m_w}{M}\right]\left[\tfrac{1}{4} + \bar{k}_w^2\right]\left[\tfrac{1}{2}(1 + \bar{W}^2)\,\bar{B}_1 + \bar{B}_2\right] \tag{A.16}$$

$$\begin{aligned} A_2 = {} & \left[\eta\,(1-\eta) + \frac{\bar{W}^2}{4} + \bar{k}^2\right]\omega_0^2 + \bar{k}^2(\bar{K}_1 + \bar{K}_2) \\ & + (1-\eta)^2\bar{K}_2 + \eta^2\bar{K}_1 + 2\,\bar{B}_1\bar{B}_2 \\ & + \tfrac{1}{4}\left[\frac{m_w}{M}\right]^2\left[\tfrac{1}{4} + \bar{k}_w^2\right]\omega_0^2(1 + \bar{W}^2) \\ & + \tfrac{1}{2}\left[\frac{m_w}{M}\right]\left[\tfrac{1}{4} + \bar{k}_w^2\right]\left\{\left[(1 + \bar{W}^2)\omega_0^2 + (1 + \tfrac{1}{2}\bar{W}^2)(\bar{K}_1 + \bar{K}_2)\right]\right\} \\ & + \tfrac{1}{2}\left[\frac{m_w}{M}\right]\omega_0^2\left[\bar{k}^2 + \tfrac{1}{2} - \eta\,(1-\eta) + \frac{\bar{W}^2}{4}\right] \end{aligned} \tag{A.17}$$

$$A_1 = \tfrac{1}{2}\bar{B}_1\,[\,\bar{K}_1 + \bar{K}_2 + \omega_0^2(1+\bar{W}^2)\,]$$
$$+ \bar{B}_2\,(\omega_0^2 + \bar{K}_1 + \bar{K}_2\,)$$
$$+ \tfrac{1}{2}\left[\frac{m_w}{M}\right]\left[\tfrac{1}{2}\bar{B}_1(1+\bar{W}^2) + \bar{B}_2\right]\omega_0^2 \qquad \text{(A.18)}$$

$$A_0 = [\eta(1-\eta) + \frac{\bar{W}^2}{4}]\omega_0^4$$
$$+ [(\eta + \frac{\bar{W}^2}{4})\bar{K}_1 + (1-\eta+\frac{\bar{W}^2}{4})\bar{K}_2\,]\omega_0^2 + \bar{K}_1\bar{K}_2$$
$$+ \tfrac{1}{16}\left[\frac{m_w}{M}\right]^2\omega_0^4(1+\bar{W}^2)$$
$$+ \tfrac{1}{4}\left[\frac{m_w}{M}\right]\omega_0^2\left[\,(1+\bar{W}^2)\omega_0^2 + (1+\tfrac{1}{2}\bar{W}^2)(\bar{K}_1+\bar{K}_2)\right] \qquad \text{(A.19)}$$

where ω_0 is the simple pendulum frequency of M, as defined by:

$$\omega_0^2 = g/H \qquad \text{(A.20a)}$$

and where:

$$\bar{K}_1 = K_1/M \qquad \text{(A.20b)}$$
$$\bar{K}_2 = K_2/M \qquad \text{(A.20c)}$$
$$\bar{B}_1 = B_1/M \qquad \text{(A.20d)}$$
$$\bar{B}_2 = B_2/ML^2 \qquad \text{(A.20e)}$$

A.3 Differentials of the Characteristic Equation

As is developed in more detail in Reference 1, differentials of the characteristic equation must be taken in order to effect the multi–variable Newton–Raphson iterative solution for the extraction of the four required mechanical properties. Essentially, the mathematical procedure is to differentiate Eq. A.14, with respect to each of the eigenvalues ($i = 1,2$) and with respect to each of the required mechanical properties:

$$(4A_4\lambda_i^3 + 3A_3\lambda_i^2 + 2A_2\lambda_i + A_1)\,\delta\lambda_i$$

$$+ \frac{\partial}{\partial(\bar{k}^2)}[A_4\lambda_i^4 + A_3\lambda_i^3 + A_2\lambda_i^2 + A_1\lambda_i + A_0]\,\delta(\bar{k}^2)$$

$$+ \frac{\partial}{\partial\eta}[A_4\lambda_i^4 + A_3\lambda_i^3 + A_2\lambda_i^2 + A_1\lambda_i + A_0]\,\delta\eta$$

$$+ \frac{\partial}{\partial\bar{B}_1}[A_4\lambda_i^4 + A_3\lambda_i^3 + A_2\lambda_i^2 + A_1\lambda_i + A_0]\,\delta\bar{B}_1$$

$$+ \frac{\partial}{\partial\bar{B}_2}[A_4\lambda_i^4 + A_3\lambda_i^3 + A_2\lambda_i^2 + A_1\lambda_i + A_0]\,\delta\bar{B}_2 = 0 \qquad \text{(A.21)}$$

Using this approach together with the details presented in the appendix of Reference 1, the R and S matrices can be formed.

A.4 Extraction of Blade Inertia Characteristics from Combined and Cradle Characteristics

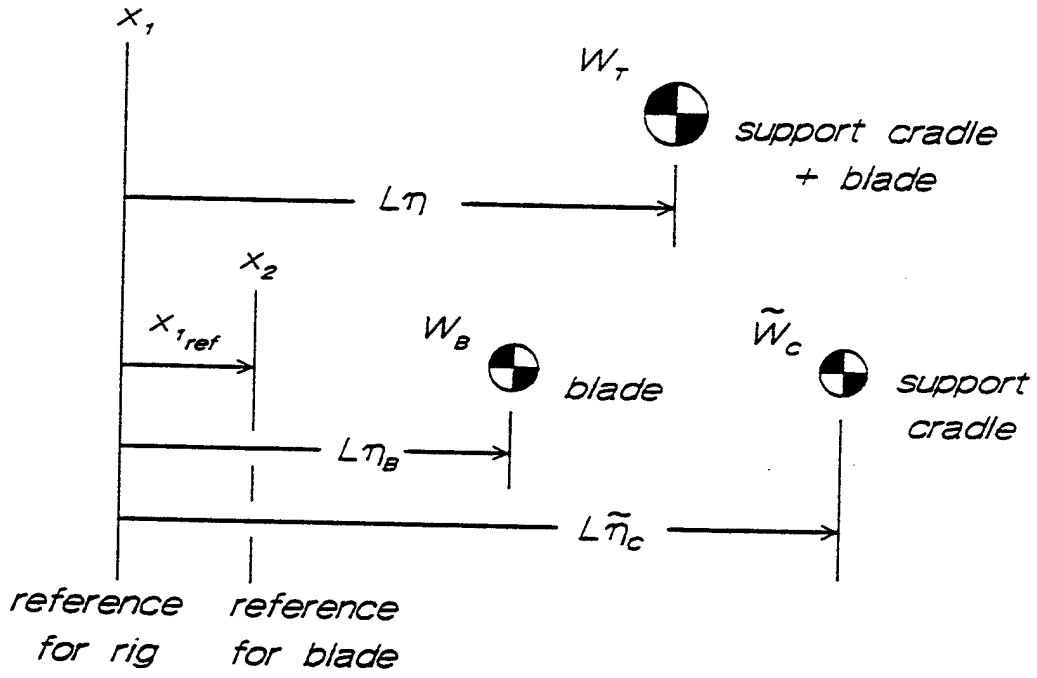

Figure A-2. Resolution of component weights and weight moments

Standard formulas can be used to calculate the first and second mass (or in this application, weight) moments of the blade (test article) from the measured properties of the cradle by itself and those of the total test inertia. First, let us include the weights of the springs; a reasonable approximation is that one half of the spring mass effectively enters into the motion defined at the spring attachment point at the cradle. Note that springs K_1 and K_2 are each physically comprised of two springs (one either side of the cradle). Thus, we denote the weights of one of each pair as W_{K_1} & W_{K_2}. These weights then add to the cradle weight, and first and second weight moments:

$$\tilde{W}_C = W_C + W_{K_1} + W_{K_2} \tag{A.22}$$

$$L\,\tilde{\eta}_C = \frac{1}{\tilde{W}_C}(S_{x_{1C}} + W_{K_2}) \tag{A.23}$$

$$\tilde{I}_{zz_{1C}} = I_{zz_{1C}} + L^2 W_{K_2} \tag{A.24}$$

1) **Blade weight**

$$W_B = W_T - \tilde{W}_C \tag{A.25}$$

2) **Blade static moment:**

$$L\,\eta_B\,W_B + L\,\tilde{\eta}_C\,\tilde{W}_C = L\,\eta\,W_T \tag{A.26}$$

Note that $L\eta_B W_B = S_{x_{1B}}$ and $L\tilde{\eta}_C \tilde{W}_C = \tilde{S}_{x_{1C}}$, therefore:

$$S_{x_{2B}} = L\,\eta\,W_T - \tilde{S}_{x_{1C}} - x_{1_{ref}} W_B \tag{A.27}$$

3) **Blade second weight moment:**

$$I_{zz_{1B}} + \tilde{I}_{zz_{1C}} = W_T(\bar{k}^2 + \eta^2)\,L^2 \tag{A.28a}$$

Therefore:

$$I_{zz_{1_B}} = W_T(\bar{k}^2 + \eta^2) L^2 - \bar{I}_{zz_{1_C}} \tag{A.28b}$$

and, upon substitution, the blade inertia about the $x_{1_{ref}}$ point can then be written as:

$$I_{zz_{2_B}} = I_{zz_{1_B}} - 2\, x_{1_{ref}} (L\, \eta\, W_T - \bar{S}_{x_{1_C}}) + x^2_{1_{ref}} W_B \tag{A.29}$$

where $x_{1_{ref}}$ is the distance between the carriage reference, which is arbitrarily taken to be the location of the cable attachments, and the reference location defined for the blades (i.e., the location of the root retention pin centers.